

AD-A256 906



①

DTIC
ELECTE
OCT 23 1992
S C D

Meridional Circulation in the Tropical North Atlantic

Marjorie A. M. Friedrichs

MIT/WHOI Joint Program
August, 1992

UNCLASSIFIED STATEMENT A
Approved for public release
Distribution Unlimited

92-27774



2P8

15

MERIDIONAL CIRCULATION IN THE TROPICAL NORTH ATLANTIC

by

MARJORIE ANNE MACWHORTER FRIEDRICHS

B.A., Middlebury College, 1989

submitted in partial fulfillment of the requirements for the degree of

MASTER OF SCIENCE

at the

MASSACHUSETTS INSTITUTE OF TECHNOLOGY

and the

WOODS HOLE OCEANOGRAPHIC INSTITUTION

September, 1992

© Marjorie A. M. Friedrichs, 1992
All rights reserved

The author hereby grants to MIT and WHOI permission to reproduce and distribute copies of this thesis document in whole or in part.

Signature of Author Marjorie A. M. Friedrichs
Joint Program in Physical Oceanography
Massachusetts Institute of Technology/
Woods Hole Oceanographic Institution

Certified by Melinda M. Hall
Dr. Melinda M. Hall
Thesis Supervisor

Certified by Lawrence J. Pratt
Dr. Lawrence J. Pratt
Chairman, Joint Committee for Physical Oceanography

Accession For	
NTIS GRAB	<input checked="" type="checkbox"/>
ERIC TAB	<input type="checkbox"/>
Unannounced	<input type="checkbox"/>
Justification	
by Res Form 50	
Distribution/	
Availability Codes	
Dist	Special
A-1	



Meridional Circulation in the Tropical North Atlantic

by

Marjorie A. M. Friedrichs

Submitted to the Joint Program in Physical Oceanography
Massachusetts Institute of Technology
Woods Hole Oceanographic Institution
on August 19, 1992, in partial fulfillment of the
requirements for the degree of Master of Science

Abstract

A transatlantic CTD/ADCP section nominally located at 11°N was carried out in March 1989. In this paper relative geostrophic velocities are computed from these data via the thermal wind balance, with reference level choices based primarily on water mass distributions. Mass is conserved by requiring the geostrophic transport to balance the sum of the Ekman and shallow western boundary current transports.

A brief overview of the meridional circulation of the upper waters resulting from these analysis techniques is presented, and indicates a North Brazil Current transport of nearly 12 Sv. Transports of the shallow waters are found to support the results of Schmitz and Richardson (1991) who found nearly half of the Florida Current waters to be derived from the South Atlantic. Schematic circulation patterns of the NADW and AABW are also presented. The deep waters of the western basin are dominated by a cyclonic recirculation gyre, consisting of a southward DWBC transport of 26.5 ± 1.8 Sv, with nearly half of this flow returning northward along the western flank of the MAR. A particularly notable result of the deep western basin analysis is the negligible net flow of middle NADW. Although the northward flows of upper and lower NADW along the western flank of the MAR are believed to be associated with the local recirculation gyre, the northward flow of middle NADW, which nearly balances the southward flow of this water mass along the western boundary, may be derived from the eastern basin of the South Atlantic. The deep waters of the eastern basin are also dominated by a large cyclonic recirculation gyre, consisting primarily of lower NADW and supplemented by middle NADW and AABW. Each of these water masses, as well as the upper NADW, have small net northward flows within the eastern basin. The AABW most likely enters the eastern basin by means of the Vema Fracture Zone, while the lower NADW enters primarily through the Kane Gap.

Although the components of the horizontal circulation discussed above agree well with results from previous CTD, current meter, and float studies, the meridional overturning cell (5.2 ± 1.6 Sv) and the net heat flux ($2.3 \pm 1.6 \times 10^{14}$ W) calculated in this study are considerably lower, and the net freshwater flux (-0.60 ± 1.5 Sv) is slightly higher than previous estimates. These discrepancies may be attributed to: (1) differences in methodologies, (2) the increased resolution of this section (as compared to earlier IGY sections), and (3) temporal (including decadal, synoptic, and most importantly, seasonal) variability. Annual average meridional overturning (12 Sv), heat flux (11×10^{14} W), and freshwater flux (-0.35 Sv), are computed based on annual average Ekman and NBC transports, temperatures, and salinities, and agree well with most previous annual estimates. The large difference between the March and the annual estimates is indicative of the importance of seasonal variability within the tropical North Atlantic.

Thesis Supervisor: Melinda M. Hall
Title: Associate Scientist



Acknowledgments

I am grateful to my thesis advisors Mindy Hall and Harry Bryden for helpful suggestions made throughout this work. I would also like to thank my other committee members, Breck Owens, Paola Rizzoli, Phil Richardson, and Nelson Hogg, for useful comments on the final drafts of this thesis. Stimulating conversations with Mike McCartney throughout the entire past year are also gratefully acknowledged. This work has been supported by the Office of Naval Research through the American Society for Engineering Education.



Table of Contents

1. Introduction	9
2. Data and Analysis Techniques	
a. Data	11
b. Ekman and shallow western boundary current transport	12
c. Reference levels	
1) Application of historical reference levels	13
2) Reference levels used in this study	15
3. Results	
a. Horizontal circulation	19
1) Shallow waters: $\theta > 4.7^{\circ}\text{C}$	20
2) Deep waters: $\theta < 4.7^{\circ}\text{C}$	23
b. Meridional transports	29
1) Volume transport	30
2) Heat transport	30
3) Freshwater transport	32
4. Discussion	
a. Methodology	35
b. Data resolution	36
c. Temporal variability	
1) Decadal	37
2) Synoptic	37
3) Seasonal	38
5. Summary	42
Appendix	45
References	49
Tables	53
Figures	59



1. Introduction

One of the best ways of examining large scale oceanic circulation, and a proven method of directly computing meridional heat and freshwater fluxes, is the analysis of zonal coast to coast hydrographic sections. The data previously used for such studies in the Atlantic have primarily been the International Geophysical Year (IGY) data of the 1950's (Hall and Bryden 1982; Roemmich 1983; Roemmich and Wunsch 1985; Rintoul 1991). Although these sections can give us some insight as to the net mass, heat, and freshwater transports in the Atlantic, the poor horizontal (and vertical) resolution of these transects makes it difficult to identify the nature of the horizontal circulation.

In this study we reexamine the circulation of the tropical North Atlantic by analyzing a much more recent hydrographic section nominally located at 11°N. As a result of the high horizontal resolution of this section (four to five times greater than that of the IGY transects), a detailed analysis of the horizontal circulation across this section is possible. Thus, a primary goal of this study is to quantify some of the known circulation patterns in the tropical Atlantic, such as the magnitude of the Deep Western Boundary Current (DWBC) and its recirculation, as well as bring to light new elements of the circulation such as the possible net northward flow of middle North Atlantic Deep Water (NADW). Comparison between the horizontal circulation results of this study and those from other float, current meter, and CTD data analyses helps us to paint a definitive picture of the meridional flow patterns in this region.

Since this transect reaches all the way from French Guiana to Senegal, direct computations of heat and freshwater transports are also possible. Partly as a result of the lack of direct heat flux estimates (there have only been a couple direct computations of heat flux (Roemmich 1983; Wunsch 1984) in the tropical North Atlantic), heat transport estimates obtained indirectly via surface heat budgets and general circulation models vary widely. Although integrations of evaporative fluxes provided by Baumgartner and Reichel (1975) and Schmitt et al. (1989) indicate a maximum of freshwater transport in the tropical North Atlantic (Wijffels et al. 1992), freshwater transport has never been directly calculated within this region. Therefore an important part of this paper will be to provide direct estimates of heat and freshwater fluxes with which the many indirectly calculated fluxes can be compared.

The tropical North Atlantic is particularly complicated by the strong seasonal variability of the winds (and the resulting Ekman transport) and the North Brazil Current (NBC). Although the horizontal circulation patterns of the intermediate, deep and bottom waters are relatively independent of the Ekman and western boundary current transports, the strength of the meridional overturning cell is extremely dependent on these factors. As a result, the net volume, heat and freshwater fluxes are highly sensitive to seasonal changes. From previous observational studies we can approximate the Ekman and NBC transports at other times of the year, and thus we are also able to estimate the magnitude of the seasonal variability in these net meridional fluxes. Although it is more difficult to assess, the possibility of decadal variability (between for instance the 1950's IGY data and our 1989 section) will also be discussed.

In this study, volume, heat, and freshwater transports are calculated by integrating velocities obtained by means of the dynamic method. Since such geostrophic calculations determine only vertical shear, and not absolute velocities, one needs to know the absolute velocity a priori at one depth for each station pair in order to determine absolute velocities. There are a number of ways in which the velocity at such a 'reference level' can be determined. If long-term current meter records or acoustic doppler current profiler (ADCP) measurements are available in the vicinity of the hydrographic stations, the geostrophic velocities can, in theory, be referenced to these absolute velocities. Beta spiral and inverse methods can also be used. Although some of these other methods may be applied to this data set in the future, in this paper we use the more traditional method of choosing a level (or levels) of no motion based primarily on water mass distributions and using these as a reference for the geostrophic velocity calculations. Mass conservation is then satisfied by balancing the geostrophic transport with the sum of the shallow NBC transport and the ageostrophic Ekman transport. The consistency of our results with available direct velocity measurements and other CTD studies in the area justifies our analysis methods a posteriori.

In the next section we provide a brief description of the data used in this study, followed by a discussion of some of the subtleties in the data analysis. In section 3 the horizontal circulation across this transect is described and the net heat and freshwater fluxes are calculated. Possible explanations for the relatively low values we obtain for these latter fluxes, in comparison to other direct, indirect and model estimates, are discussed in Section 4. Section 5 contains a brief summary.

2. Data and Analysis Techniques

a. Data

In March 1989, D. Roemmich, M. Hall, and T. Chereskin carried out a CTD/hydrographic/ADCP zonal section across the tropical North Atlantic Ocean, repeating the track of a basin-wide deployment of SOFAR (Sound Fixing and Ranging) floats completed by P. Richardson and W. Schmitz the previous month. The 4000 km cruise track, shown in Figure 1, consisted of 84 CTD stations, each of which extended from the surface down to within 10 m of the bottom. The average station spacing was 50 km, with shorter spacing of 15 - 25 km near the coasts and in regions of strongly variable topography. Beginning at the 200 m isobath off Senegal, the ship angled slightly southwestward for a short segment before heading due west along $11^{\circ}12'N$. In order to approach the South American coast perpendicularly, the ship made a second turn toward the southwest at roughly $46.5^{\circ}W$. The last station was located near the 200 m isobath off French Guiana. To the west of this CTD, the ADCP was used in bottom-tracking mode in order to determine the transport of the NBC over the wide shallow shelf, illustrated in Figure 2.

Although later work on this project will synthesize the hydrographic data with the SOFAR float and ADCP data, in this work we employ the traditional method of choosing a reference level based primarily on water mass distributions, and referencing the geostrophic velocity calculations to this assumed level of least motion. When using this method there are a number of choices that must be made. For instance, one must decide what velocity to attribute to the bottom triangles, and how to account for intervening topography. (The details of this part of the analysis are given in the Appendix.) The Ekman and shallow western boundary transports must also be computed using either climatological data or in situ ADCP data obtained during the cruise. A reference level, or combination of reference levels, must also be chosen in order to obtain absolute velocities from the relative velocities given by the application of the thermal wind relationship. All these choices must be made in such a manner that mass is conserved, i.e. total geostrophic mass transport across the section must balance the shallow western boundary and Ekman transports. The remainder of this section describes ways in which these complications have been addressed in the past, as well as how they are specifically dealt with in this study.

b. Ekman and shallow western boundary transport

Ekman transport is a major component in the meridional circulation, heat and freshwater balances of the tropical North Atlantic. For example, using IGY 8°N data, Roemmich (1983) found the heat flux due to the Ekman transport to be greater in magnitude than that due to the geostrophic transport. This condition was not found at the sections Roemmich examined at 24°N, 8°S and 24°S.

Chereskin and Roemmich (1991) computed the Ekman transport across the 11°N transect (to the east of the first CTD located at the 200 m isobath) using three different methods. The difference between the geostrophic shear and the shear measured by the ADCP data yielded an estimate of 12.0 ± 5.5 Sv and is in good agreement with that estimated from the shipboard winds, 8.8 ± 1.9 Sv. Using the mean monthly winds of Hellerman and Rosenstein (1983) for the month of March, they obtained a third estimate of 13.5 ± 0.3 Sv. Since the cruise period was characterized by particularly low winds, it is not surprising that the calculations using the in situ data yielded smaller estimates of Ekman transport. In this examination of the March 1989 circulation across 11°N, the best estimate of Ekman transport is assumed to be a weighted mean of the two in situ estimates: 9.1 ± 1.8 Sv. In order to yield a more accurate representation of the circulation for March in general, calculations using the climatological estimate will also be shown where appropriate.

Along the western boundary of this transect, the northwestward flow of the NBC is evident from the data of the shallowest few CTD's. Using the ADCP in bottom tracking mode, this $O(1 \text{ m}\cdot\text{s}^{-1})$ flow was observed to extend across the wide shallow shelf where no CTD data was taken (Chereskin and Roemmich 1991). (See Figure 2.) The across track component of the flow between the coast and the first CTD station, i.e. the 200 m isobath, is hereafter referred to as the 'shallow NBC transport'. Using the ADCP data over the shelf, Chereskin (pers. comm.) calculated the net shallow NBC transport to be 4.5 ± 1 Sv. Absolute velocities were integrated from the bottom to 30 m (2.7 Sv), and a slab extrapolation was applied between 30 m and the surface (1.8 Sv). Of this net flow, 3.3 Sv was found to be in water depths of less than 100 m, in good agreement with the shallow transports of the North Brazil Current obtained by Candela et al. (1992) using ADCP and CTD data from March 1990.

The remaining calculations in this paper are performed assuming that the geostrophic component of the flow (to the east of the first CTD) must balance the sum of the net northward Ekman transport and the shallow western boundary transport, i.e. 13.6 ± 2.1 Sv. Error bars on the geostrophic transports will include the propagation of the uncertainty in this sum.

c. Reference levels

1) APPLICATION OF HISTORICAL REFERENCE LEVELS

Selecting a reference level of no motion is a fundamental aspect of transport analyses based on geostrophic velocity calculations; a change in reference level of only a few hundred meters can sometimes change even the sign of the net transport across a hydrographic section. It is common practice to examine property distributions across hydrographic sections, and to choose reference levels of no motion between known water masses flowing in opposite directions. Using seven IGY sections in the Atlantic, Wright (1970) chose a reference level which approximated the boundary between the NADW and the AABW. This boundary was determined by examining temperature-depth and salinity-depth profiles, and selecting the level where a discontinuity in the profiles occurred. The result of this analysis was a reference level that sloped from roughly 4400 m at the 16°N section to 3400 m at the 32°S section, and nominally coincided with the 1.9°C isotherm. (All temperatures throughout this paper refer to *potential* temperatures.) In their study in the vicinity of the Greater Antilles Outer Ridge north of Puerto Rico, Tucholke et al. (1973) experimented with a reference level of 4700 m, also roughly approximating the boundary between the NADW and the AABW. A level of no motion at $\theta = 1.9^\circ\text{C}$ was also used by Whitehead and Worthington (1982) (as well as by McCartney (1992a) in a recent update of their analysis) for a group of hydrographic stations in a 300 km wide gap at 4°N between the Mid-Atlantic Ridge (MAR) and the Ceara Rise.

Reference levels have also been chosen in the upper water column. In his comprehensive dynamic calculations using six Meteor sections, Wust (1955; 1957) was one of the first to choose an intermediate reference level. His choice was based on an approximation of the boundary between the Antarctic Intermediate Water (AAIW) and the upper NADW, and sloped from less than 1000 m at 19°N to about 2000 m at 33°S. More recently, Molinari et al. (1992) have found the 4.7°C isotherm to be a useful approximation to the level of no motion in their examination of the DWBC in the western tropical North

Atlantic. Bennett and McCartney (1990) also suggest "fairly unambiguous choices for levels of no motion" to be between the 4° and 5°C potential temperature surfaces in this region of the Atlantic Ocean.

As discussed above, in past hydrographic studies of the tropical Atlantic, a single reference level was often chosen to approximate either (1) the boundary between lower NADW and AABW (roughly 4500 db or $\theta \approx 1.8 - 1.9^\circ\text{C}$) or (2) the boundary between AAIW and upper NADW (roughly 1200 db or $\theta \approx 4.7^\circ\text{C}$). For comparison, both of these reference levels are applied to the full 11°N section, and the transport results for different water masses are shown in Figure 3. Isothermal boundaries for the water masses are determined from the θ -S diagrams shown in Figure 4. Corresponding definitions of water masses are listed in Table 1. Station pairs which include at least one station shallower than the reference level are referenced to the deepest common level. In each case mass is balanced by requiring the geostrophic transport to be equal and opposite to the sum of the Ekman and shallow NBC transports. This is done by adding a small uniform velocity, v_0 , across the entire section, thus changing the reference level from a level of 'no' motion to a level of 'known' motion, i.e. v_0 , and simultaneously shifting the zero velocity surface to a slightly different depth. Error bars on the transports in Figure 3 are based on the uncertainties in the bottom triangle transports (see Appendix), as well as in the sum of the Ekman and shallow NBC transports.

Although a deep reference level can sometimes give reasonable results (Wright 1970; Tucholke et al. 1973; Whitehead and Worthington 1982; McCartney 1992a), it appears that this is probably not the best possible approximation to the level of no motion at 11°N. As a result of the rather large mass imbalance of 38 Sv caused by choosing (initially) 4500 db to be a level of no motion, a uniform velocity of $v_0 = -0.21$ cm/s must be added to the section. This is equivalent to raising the average level of no motion by 1000 db which places it in the center of the lower core of NADW! As expected, results from such a calculation, as shown in Figure 3a, show very little NADW flowing south. (If a 1.8°C isothermal reference level had been used in place of the 4500 db isobaric reference level, the net NADW transport would be northward.) Equally problematic is the relatively large *southward* flow of AABW caused by the use of this deep reference level.

As described above, shallow reference levels approximating the boundary between the AAIW and the upper NADW have also frequently been used in the tropical North Atlantic (Wust 1955; Wust 1957; Molinari et al. 1992; Bennett and McCartney 1990). The mass imbalance caused by a reference level of 1200 db is considerably smaller, and

requires a velocity of only $v_0 = 0.08$ cm/s to be added uniformly to the section. The addition of such a small velocity changes the level of no motion by less than 20 m and immediately indicates that this reference level choice is likely to give more reasonable results. However, Figure 3b only shows a slightly larger southward transport of deep water, and once again an anomalously large southward transport of AABW. Such circulation patterns lead us to continue our search for a more appropriate reference level.

2) REFERENCE LEVELS USED IN THIS STUDY

The possibility of other more carefully chosen reference levels producing more realistic transports of AABW and NADW is now considered. Figure 5 shows the total transport of AABW and NADW plotted as a function of reference level. For each reference level shown, a velocity v_0 has been added uniformly to the entire section in order to maintain mass conservation. It is important to note that if a constant reference level is chosen across the entire section, the maximum possible northward flow of AABW is 0.4 Sv. This is considerably smaller than previous estimates of transequatorial bottom water transport which exceed 4 Sv (McCartney and Curry 1992; McCartney 1992a). Furthermore, if the AABW is required to flow northward, the resulting transport of total NADW is still only between 4 and 5.5 Sv. This is a surprisingly low value, since deep water transports of roughly 17 Sv have been found both at 24°N (Hall and Bryden 1982) as well as at 32°S (Rintoul 1991).

Although Figure 5 shows the transport results for a number of different reference levels, the realm of possible reference level choices is not yet exhausted. In the analysis above, a single reference level was chosen to best approximate the level of least motion for all station pairs. In an attempt to determine whether the small northward transport of AABW and the small southward transport of NADW found above are real or are simply artifacts of using a constant reference level across the entire section, we now allow for the possibility that different regions of the 11°N transect may have different levels of no motion. (In fact, it is likely that each station pair has a different level of no motion; however, due to the limited number of known constraints, it is only possible to rationalize the use of a few different reference levels.) As a result, the western and eastern basins will now be examined separately. Since more previous work has been carried out in the western basin than in the eastern basin, the discussion of reference level choice will begin there.

Numerous studies in the past few decades indicate that the circulation within the western basin of the tropical North Atlantic varies tremendously from west to east. On the eastern side the AABW flows northward (McCartney 1992a), while on the western side the NADW flows southward along the Brazil coast (Johns et al. 1992a; McCartney 1992b). Furthermore, the core of the upper NADW is typically found inshore of the core of lower NADW (Molinari et al. 1992). Thus it is conceivable that the best approximation to the level of no motion may also differ considerably across the western basin. Therefore, the western basin is divided into three subsections with different reference levels allowed within each region.

One reasonable location to subdivide the western basin is at the abrupt change in topography and increase in depth near 46.5°W (or equivalently ~ 850 km offshore of the shelf break) where the cruise track slightly changes direction, as shown in Figure 1. This division is illustrated in Figure 6 and is reinforced by observations which indicate that in the tropical North Atlantic the NADW extends at least 800 km offshore (Molinari et al. 1992). Furthermore, within the deep waters of the 11°N transect the highest values of dissolved oxygen and the lowest values of silicate and phosphate, which are indicative of the NADW, lie primarily in the westernmost 850 km as illustrated in Figure 7. A second division of the basin is imposed in order to allow the upper and lower cores of NADW to have different reference levels. A division positioned near 50°W (or equivalently ~ 175 km offshore of the shelf break, as shown in Figure 6) appears to separate the inshore core of upper NADW at 1800 m depth from the offshore core of lower NADW. Such a boundary is also useful in that it marks the location of a significant change in the bottom slope. It must be remembered, however, that such divisions are primarily convenient methods by which reference level possibilities can be examined. Even if such separations existed they probably would not be uniform with depth, but might be tilted with the slope of the surrounding bathymetry.

Since logical divisions between the eastern, middle and western parts of the west basin have now been established, the reference levels must be decided upon for each of these regions. One method of determining a level of least motion is to examine current meter data. There are two sets of current meter data off the coast of S. America that are relevant to our 11°N section: Whitehead and Worthington's array at 4°N , and the array of Johns et al. (1992a) at 8°N . (Because neither of these arrays were coincident in time or space with our section, it is not logical to reference our geostrophic velocities directly to these current meter measurements.) Since all the current meters at 4°N are below 4000 m,

it is not possible to determine from these data alone whether a shallow or a deep level of no motion would be more appropriate. However, these data do indicate that at depths of 4000 m or so there is a strong periodic variability with roughly a 60-day time scale and amplitudes of up to 20 cm/s. The data at 8°N also show considerable vertical excursion of isotherms with a similar periodic oscillation. In some instances, AABW as cold as 1.4°C was observed to flow southward. The strong temporal variability of NADW and AABW transports at these locations introduces some doubt as to whether a reference level between these two water masses is the best choice for the western side of the western basin.

Another reason to exclude the deep reference levels from consideration in the western basin is that this part of the 11°N section crosses the hypothesized Guiana Abyssal Gyre (McCartney 1992b; Johns et al. 1992a). It is believed that within the western basin of the tropical North Atlantic, the bottom water flows northward along the MAR and returns southward along the western boundary, while the deep water flows southward along the western boundary and recirculates back northward along the western side of the MAR. This recirculation of both the NADW and the AABW appears to extend southward to the Ceara Rise (~4°N) and northward to at least 14°N (Molinari et al. 1992). Thus it is likely that within the entire western basin the AABW is flowing in the same direction as the lower NADW, and a reference level between these water masses is not suitable as a level of no motion.

Evidence of the Guiana Abyssal Gyre is shown in the potential temperature contours of Figure 7a. Here the isotherms both above 1.8° (NADW) and below 1.8° (AABW) slope upward toward the coast. If a reference level of $\theta = 1.8^\circ\text{C}$ is chosen, the resulting NADW flow would be *northward* - in disagreement with almost all tracer and current meter data in the DWBC. Furthermore, although the strong maximum of dissolved oxygen provides indisputable evidence for the presence of NADW (Figure 7c), this maximum is associated with isotherms ($\theta = 1.8^\circ - 2.4^\circ\text{C}$) rising towards the western boundary; these are indicative of a southward flowing water mass only if a reference level above the lower core of NADW (i.e. shallower than 3000 db) is chosen. Similarly on the eastern side of the western basin, the high silicate values of the AABW (Figure 7d) lie near the bottom of the western basin and are coincident with isotherms ($\theta = 1.4^\circ - 1.9^\circ\text{C}$) sloping upward against the MAR; these are indicative of a northward flowing water mass only if a reference level above 3000 db is chosen.

Although deep reference levels have now been eliminated from consideration, which reference levels are preferable? In order to gain insight into this question, transport

per unit depth relative to the bottom is plotted in Figure 8. Transport per unit depth for the section as a whole is shown in Figure 8a, and that for the individual Regions 1 - 3 are shown in Figures 8(b, c, and d) respectively.

Figure 8b indicates two distinct water masses in Region 1: one located at 800 m depth and the other at 1800 m. The upper layer is identified as AAIW by its strong oxygen minimum (Figure 7c), while the silicate maximum of the lower core (Figure 7d) indicates that it must be of northern origin. Because the long term mean flows of these two water masses are expected to be in opposite directions, a reference level of 1100 db is chosen.

Figures 8c and 8d do not show any clear levels of least motion and thus a different method must be used to determine the reference levels for Regions 2 and 3. Since deep reference levels have already been eliminated from consideration, only those between 1000 db and 3000 db are allowed. If reference levels of 100 db increments are considered, there are 441 possible combinations for the western basin alone. Each of these 441 combinations were examined, and those with southward flow of AABW with a magnitude greater than 0.5 Sv were rejected. Since McCartney et al. (1991) predict a northward flow of roughly 2 Sv in the western basin across 11°N, our initial constraint is a mild one; at this point we only reject absurdly large southward flows of bottom water. (Also note that mass cannot yet be balanced since a reference level for Region 4 has not yet been chosen; however, as a result of the small area that the AABW occupies, the addition of a typical v_0 ($O(+.1 \text{ cm}\cdot\text{s}^{-1})$) will increase the western basin bottom water transport by only 0.2 Sv.) This single constraint eliminates 293 combinations from further consideration.

Figure 9 illustrates the western basin NADW and AABW transport for all the possible reference level combinations discussed above. The combinations rejected due to large southward transports of AABW are shaded, and, as shown in Figure 9b, correspond to the largest southward transports of NADW. As a result of the anomalously low transports of NADW shown in Figure 5, we now select from the remaining (unshaded) 148 combinations the 20% (i.e. 30 levels) that have the greatest transport of NADW. These 30 choices are shown by asterisks in Figure 9b. (Note that after mass is balanced by uniformly adding a typical positive v_0 to the section, the southward flowing western basin NADW transport will decrease in magnitude by roughly 3 Sv.)

Eastern basin reference levels are now chosen such that total NADW transport (across the entire section) is maximized for each of these 30 combinations. All levels between 1000 db and 5000 db (in 100 db increments) are examined. For every one of the

30 combinations found above, the eastern reference level that maximizes total NADW transport (after balancing mass), is located at 2100 db.

In summary, levels of no motion have been chosen that give "reasonable" western basin AABW transport and simultaneously maximize total NADW transport. These criteria yield reference levels of 1100 db for Region 1, 2100 db for Region 4 and thirty possible reference level combinations for Regions 2 and 3, as depicted in Figure 9b, and listed in Table 2. The resulting net transports are shown in Figure 10. Error bars include the uncertainties in the bottom triangle, Ekman, and shallow NBC transports. The error due to reference level choice is assumed to be equal to the standard deviation of the thirty different reference level calculations, and in this case is insignificant in comparison to the other sources of error.

The transport results shown in Figure 10 are clearly more reasonable than the initial results shown in Figure 3. For instance, the net transport of AABW is now northward, in agreement with previous current meter, tracer and CTD data. Although the southward transport of deep water has doubled, it is still considerably smaller than that obtained in previous mid-latitude studies of IGY data (Hall and Bryden 1982; Rintoul 1991). Further discussion of the discrepancy in these results is postponed to Section 4. In the following section we first examine in detail the circulation patterns resulting from the data analysis methods described above, and compare these with other results of recent float, current meter and CTD studies.

3. Results

a. Horizontal circulation

Volume transport in seven temperature classes is computed for each of the reference level combinations described in Table 2. The results for the four different regions are shown in Figures 11 (a, b, c, and d) respectively. The error bars on these transports include the uncertainties in the bottom triangle (see Appendix), Ekman, and shallow NBC transports, as well as the error in our reference level choice which again is assumed to be equal to the standard deviation of the thirty estimates. In contrast to the net transport calculations (Figure 10), the reference level errors dominate the error bars of Figure 11. The bottom triangle errors are significant only in the AABW transports, and the uncertainties in the Ekman and shallow NBC transports are important only in the eastern

basin. Before beginning a detailed description of the deep and bottom water circulation, a brief overview of the shallow water circulation will be presented.

1) SHALLOW WATERS: $\theta > 4.7^{\circ}\text{C}$

Due to the strong temporal variability of shallow tropical waters, the circulation of the upper waters near 11°N is not well known; however, one aspect of the tropical North Atlantic circulation that has been the subject of a number of recent investigations (Candela et al. 1992; Johns et al. 1992b) is the North Brazil Current (NBC). Although this current is strongly seasonal (Cochrane 1979; Philander and Pacanowski 1986) the magnitude of the seasonal variation is not yet well defined. Recent studies indicate, however, that the NBC may range from roughly 10 Sv in the spring to as much as 30-35 Sv in the fall (Candela et al. 1992; Johns et al. 1992b). An estimate of the NBC transport, which is herein defined to include the northwestward flow of $\theta > 12^{\circ}\text{C}$ waters located within 250 km of the western boundary, can also be obtained from the 11°N section. The portion of this flow located over the 150 km wide shelf was determined from the ADCP data to be 4.5 Sv (T. Chereskin, pers. comm.), while the component of this shallow flow in deeper waters (200 m - 3000 m) was calculated from the first six CTD pairs to be 7.3 Sv. The total NBC transport is thus estimated to be 11.8 Sv, and agrees well with the recent March estimates of 10 - 15 Sv obtained by Candela et al. (1992) and Johns et al. (1992b).

In order to examine the horizontal circulation of the shallow waters in greater detail, we divide these waters into 4 temperature classes: surface water ($\theta > 24^{\circ}\text{C}$), thermocline water ($12^{\circ} < \theta < 24^{\circ}\text{C}$), lower thermocline water ($7^{\circ} < \theta < 12^{\circ}\text{C}$), and AAIW ($4.7^{\circ} < \theta < 7^{\circ}\text{C}$). The horizontal circulation of each of these temperature classes will now be examined individually.

Integrated transport of the surface water is shown in Figure 12a. The NBC is evident as a strong northwestward flowing current banked up against the western boundary and extending roughly 250 km offshore. Of the total 11.8 Sv NBC transport, 9.3 Sv is at temperatures greater than 24°C . Farther offshore an even larger 13.5 Sv southward counterflow exists. At first glance this current resembles the shallow NECC retroflection. However, a number of previous studies have shown that typically the NECC does not begin to form until May, and is nearly non-existent in March (Richardson and Walsh 1986; Philander and Pacanowski 1986). It is difficult to determine from this study alone whether this flow represents a particularly early formation (or late weakening) of the NECC, a retroflection eddy that has been pinched off from the NBC retroflection, or some

other unrelated strong southward flow. The remainder of the western basin is characterized by a 5 Sv net northward flow. The eastern basin is almost entirely composed of waters colder than 24°C. Summing the shallow NBC transport over the shelf (4.5 Sv), the Ekman transport (9.1 Sv), and the net geostrophic transport across the entire section of $\theta > 24^\circ\text{C}$ waters (-7.4 Sv), yields a net transport of surface waters across the section of 6.2 Sv. If the climatological Ekman transport value of 13.5 Sv were used (which is higher than the Ekman transport value derived from in situ data since the 11°N cruise was characterized by particularly low winds), this estimated net surface water transport would increase to 10.6 Sv.

Integrated transport of the thermocline water, shown in Figure 12b, closely resembles that of the surface water. The NBC also penetrates down to this temperature class and supplements the 9.3 Sv of $\theta > 24^\circ\text{C}$ NBC water with an additional 2.5 Sv, yielding a total NBC transport of 11.8 Sv. The southward transport offshore of the NBC that was evident in the surface water is also evident in the thermocline water, with the combined ($\theta > 12^\circ\text{C}$) transport reaching -20.3 Sv. As was the case for the surface water, the eastern portion of the western basin is dominated by a net northward flow of thermocline water, and only small net flows occur within the eastern basin. The net transport of thermocline water across 11°N is -2.6 Sv.

As shown by Figure 12c, the NBC does not penetrate down to the lower thermocline water; however, the southward flow offshore of the NBC does extend down to this temperature class (250 - 650 m) and yields a total of -25.4 Sv for this current. It is interesting to note that the magnitude of this southward flowing current is more than twice the size of the northward NBC. The flow pattern across the remainder of the section resembles that of the surface and thermocline water, with northward transport over the western side of the MAR, southward flow over the eastern side of the MAR, and only small net flows within the eastern basin. The net transport of lower thermocline water across 11°N is -0.6 Sv.

A number of the results discussed above can be compared to the results of a recent study by Schmitz and Richardson (1991). Using hydrographic data from a number of Caribbean passages as well as from the Straits of Florida, they were able to determine the origin of the surface, thermocline and lower thermocline water within the Florida Current. They found 8.9 Sv of $\theta > 24^\circ\text{C}$ water flowing northward in the Florida Current. Of this transport, they determined that only 1.8 Sv comes from the North Atlantic, and 7.1 Sv flows in from the South Atlantic. As discussed above, we find 10.6 Sv of surface water

flowing northward across the 11°N section. It is not surprising that our value is different from that of Schmitz and Richardson, since our result is representative of an average March transport (since the climatological winds have been used), while theirs is an annual average. Furthermore, it is unlikely that all the surface waters crossing 11°N are entrained into the Florida Current. In fact, if only the westernmost 1000 km (our Regions 1 and 2) are examined, a net surface water transport of 5.4 Sv is found (4.5 Sv of shallow NBC transport, -4.1 Sv of geostrophic transport, and 5 Sv of Ekman transport). This estimate is in slightly better agreement with Schmitz and Richardson's estimate of 7.1 Sv and suggests that the flow which is entrained into the Florida Current may occur primarily within the first 1000 km of the western basin.

The thermocline and lower thermocline waters provide additional evidence that most of the Florida Current waters of southern origin cross our section within the westernmost 1000 km. Within the Florida Current, Schmitz and Richardson (1991) found 13.8 Sv of thermocline water, with 13 Sv originating in the North Atlantic and 0.8 Sv coming from the South Atlantic. The net transport between $12^\circ < \theta < 24^\circ\text{C}$ crossing our 11°N section is -2.6 Sv (southward), again in support of a North Atlantic origin for this water class. Furthermore, if the thermocline water is examined only within the westernmost 1000 km of our section, we find a net northward transport of 0.2 Sv which is in reasonable agreement with the 0.8 Sv estimate of Schmitz and Richardson.

The same general pattern occurs in the $7^\circ < \theta < 12^\circ\text{C}$ water. For this temperature class Schmitz and Richardson (1991) found 6.1 Sv flowing in the Florida Current, 5 Sv of which originated in the South Atlantic. The net transport of lower thermocline water across our 11°N section is -0.7 Sv -- a value which is much smaller than, and of the opposite sign to that predicted by Schmitz and Richardson. However, the northward flow of 4.7 Sv within the westernmost 1000 km (see Figures 11(a,b)) is consistent with the 5 Sv expected by Schmitz and Richardson to cross the equator and enter the Florida Current. Further examination of our data yields another equally valid possibility: the 4.7 Sv may locally recirculate (instead of continuing northward into the Florida Current), and return 3.9 Sv southward along the western side of the MAR (see Figure 11c). From our data alone it is impossible to distinguish between these two possibilities.

Very little is known about the circulation and transports of AAIW. As Schmitz and McCartney (1992) state: "The circulation of Antarctic Intermediate Water is virtually unexplored..." As a result, there are few other estimates of AAIW with which our results can be compared. Furthermore, the strong eddy activity characterizing this water mass

causes the AAIW transports to be extremely sensitive to the horizontal limits of integration. In Figure 11, for example, the transports of AAIW which indicate an anticyclonic circulation within the western basin, are primarily an artifact of the specific divisions we have chosen between Regions 1 - 3. This is evident from Figure 12d, which shows little evidence of such a well-defined anticyclonic flow pattern. Figures 11d and 12d indicate considerable eddy activity with only small net transports of AAIW within the eastern basin. This is consistent with the salinities found at 800 m in the eastern basin, which are slightly higher than those found at similar depths within the western basin (see Figure 7b).

One of the few studies that yield AAIW transport estimates with which our results can be compared, is that of Richardson and Schmitz (1992). They present results for neutrally buoyant SOFAR floats which were deployed at nominal depths of 800 m along the cruise track of our 11°N section. Within 200-300 km of the western boundary the floats were dominated by a northwestward along-boundary transport. The transport per unit depth of these floats, when integrated seaward from the western boundary, reached a maximum of $5.8 \pm 1.8 \times 10^3 \text{ m}^2 \cdot \text{s}^{-1}$ roughly 300 km offshore. A similar integration of our CTD data at depths between 700 and 900 m yields a maximum transport per unit depth of $7 \times 10^3 \text{ m}^2 \cdot \text{s}^{-1}$, in good agreement with the value of Richardson and Schmitz (1992).

2) DEEP WATERS: $\theta < 4.7^\circ\text{C}$

In comparison with the AAIW, the NADW is a rather well studied water mass. As early as in the 1930's (Wüst 1935) the NADW was found to have three cores, each with its own distinct characteristics and formation site. Wüst identified the upper NADW by a deep salinity maximum and attributed this to the Mediterranean outflow. He also found the middle NADW to contain a maximum in dissolved oxygen concentration which he traced back to the Labrador Sea. He believed that the lower NADW, characterized by a second, deeper oxygen maximum, was formed by deep winter convection in the region south of Greenland.

More recent studies have supported the existence of the three NADW cores, which have now been found to be most clearly identified by means of the chlorofluorocarbon F11 (Molinari et al. 1992). The upper NADW is characterized by a maximum in F11, below which lies a relative minimum of F11 associated with the middle NADW. A second F11 maximum identifies the lower NADW. For the purpose of this study, the three layers of NADW have been defined by the isotherms corresponding to the bounds Molinari et al. (1992) found on the F11 layers they observed in the western tropical Atlantic. (See Table

1.) The circulation of each of these three NADW cores as well as that of the AABW will now be discussed in succession.

Although the general trends of the upper NADW circulation can be seen from the bar graphs of Figure 11, the details of the horizontal circulation become clearer if the integrated transport of the upper NADW (Figure 12e) is examined. Here we see the strong southward flow of upper NADW banked up against the western boundary. Between 300 and 800 km offshore there appears to be a considerable amount of eddy activity, with only a small additional transport of upper NADW. Half of the upper NADW appears to recirculate back northward in a very narrow current located directly over the deepest part of the western basin. The remainder of the western basin is characterized by a small southward flow over the western side of the MAR, and a small northward return flow is evenly distributed over the eastern basin.

A schematic of the upper NADW circulation appears in Figure 13a. At 11°N the upper core of the Deep Western Boundary Current (DWBC) is shown to have a magnitude of 12 Sv. Since half of this transport appears to recirculate northward, the net southward flow of upper NADW is only 6 Sv. Although at certain times this current may continue southward across the equator, at other times it may veer eastward along the equator as shown by the recent SOFAR float data of Richardson and Schmitz (1992). Another interesting feature of the upper NADW circulation is the 2 Sv southward flow occurring along the western side of the MAR. Half of this transport may flow eastward through the Vema Fracture Zone (M. McCartney pers. comm.), while the remainder may continue southward and eventually become entrained either into the eastward flow along the equator, or into the southward flow along the western boundary (Richardson and Schmitz 1992; McCartney 1992b). The remainder of the section is characterized by a small net northward transport of 3 Sv distributed evenly over the eastern basin.

Although the circulation patterns of upper NADW have rarely been examined within the eastern basin, a number of recent studies have concentrated on deep water transport within the western basin. For instance, after analyzing a number of hydrographic sections between 0° and 14.5°N (taken between 1987 and 1989), Molinari et al. (1992) arrived at a slightly smaller average value of -4.4 ± 2.3 Sv for the transport of upper NADW within the DWBC. Our results can also be compared with those of Speer and McCartney (1992), who also determined upper NADW transport from hydrographic data in the tropical Atlantic. Since they divided the NADW into only two layers, in contrast to our three, their definition of upper NADW differs from ours. By defining this core of NADW to include

the water near the western boundary between 1200 m and 2900 m depths, they found a transport of -16.8 Sv across 13°N and -12.6 Sv across 7°-10°N. The application of their definition of upper NADW to our data yields a transport of -11 Sv, in good agreement with their 7°-10°N estimate.

The SOFAR float data of Richardson and Schmitz (1992) also give supporting evidence for a strong southward flow of upper NADW along the western boundary. Integrating the velocities obtained from their 1800 m floats over the 100 km width of the current yielded a transport per unit depth of $-13.8 \times 10^3 \text{ m}^2\text{-s}^{-1}$. By assuming that the upper NADW extends from 900 m down to 2800 m, Richardson and Schmitz also computed a transport of -15 Sv for this current. A similar 100 km zonal integration of our CTD data between 1700 and 1900 m yields an average transport per unit depth of $-10.5 \times 10^3 \text{ m}^2\text{-s}^{-1}$, in good agreement with the analogous value obtained by Richardson and Schmitz. However, our CTD data shows that this upper core extends only between 1500 m and 2500 m. This can be most clearly seen from Figure 8b, where it is clear that 1000 m is a level of northward travelling AAIW, and *not* southward travelling upper NADW. As a result, their transport of -15 Sv is larger in magnitude than our corresponding transport (i.e. only over 100 km width) of -8 Sv. The float data of Richardson and Schmitz also yielded an estimate for the upper NADW recirculation of 5.8 Sv. This value closely matches the 6 Sv of recirculation found in this study (Figure 12e and Figure 13a); however, as a result of the large possible errors Richardson and Schmitz associated with their value, this agreement may be fortuitous.

The circulation of the middle core of NADW is similar to that of the upper core, in that it also contains a strong southward flow banked up against the western boundary. As shown in Figure 12f, the southward transport of middle NADW is located directly beneath that of the upper NADW. Within the center of the western basin the flow is extremely quiet, with almost no eddy activity and only a small net northward flow. The recirculation of the middle NADW is extremely strong with the entire southward flow along the western side of the western basin returning northward along the western flank of the MAR, causing the net flow of middle NADW within the western basin to be indistinguishable from zero. A second cyclonic recirculation is apparent within the eastern basin consisting of a small southward flowing current along the eastern side of the MAR, and a larger net northward flow evenly distributed over the remainder of the section.

Middle NADW circulation patterns are presented schematically in Figure 13b. Within the DWBC the magnitude of this water mass was found to be 5 Sv, and agrees well

with the -6.3 ± 2.1 Sv of middle NADW transport observed by Molinari et al. (1992). A comparison of this circulation pattern with that of Figure 13a illustrates that the northward return flow of middle NADW is located farther to the east than the corresponding return flow of upper NADW. The southward current along the western boundary (within the DWBC) combined with a northward current of a similar magnitude along the western side of the MAR yields zero net northward transport within the western basin.

The origin of the current flowing northward along the western flank of the MAR is not well known. As shown by the θ -S plots of Figure 4 and the nutrient data of Figure 7, the original formation site of this water mass may be the northern North Atlantic. However, it is possible that a portion of the northward flowing deep water observed in the eastern South Atlantic (Warren and Speer 1991) flows into the western basin via one (or more) of the various fracture zones in the MAR. The middle NADW may then flow northward along the western side of the MAR, thus supplementing the cyclonic recirculation gyre within the western basin. The lower F11 values (Molinari et al. 1992) and the slight relative minimum in dissolved oxygen (Figure 7c) present within the middle core of NADW also support our hypothesis that at one time this water mass has been resident within the South Atlantic, and is thus slightly older than its upper and lower counterparts.

As illustrated in Figure 12f, a rather curious aspect of the middle NADW circulation is the net northward transport of this water mass across our 11°N section. This rather robust result of our study (i.e. relatively independent of reference level and Ekman transport choices) is caused by the negligible net flow within the western basin combined with a small net northward flow within the eastern basin. A possible circulation pattern for the eastern basin is presented schematically in Figure 13b. Roughly 1 Sv of the northward flowing current banked up against the western side of the MAR may flow eastward through the Vema Fracture Zone (McCartney pers. comm.). Additional middle NADW was observed to flow northward across 11°S (Warren and Speer 1991) and may continue northward through the Kane Gap and also become entrained into this recirculation gyre. Partly as a result of the local topography (i.e. the Sierra Leone Ridge and the Cape Verde Islands) 1 Sv of this flow recirculates cyclonically within the eastern basin and is accompanied by a 2 Sv net throughflow along the eastern side of the MAR. Evidence of this western intensification of the middle NADW within the eastern basin is shown in the nutrient data of the recent subtropical Atlantic sections of Roemmich and Wunsch (1985). Here properties generally associated with the NADW (such as low phosphate and high

oxygen) are found intensified over the eastern flank of the MAR at both 24°N and at 36°N. Unfortunately, since most previous deep circulation studies have been carried out within the western basin and furthermore since the NADW frequently has been divided into only two layers, there are few previous transport estimates with which these proposed circulation patterns can be compared.

The integrated transport of lower deep water is shown in Figure 12g. There is obviously much variability in this lower NADW, and the southward flow is not as western intensified as it was for the upper and middle NADW cores. The net southward transport of lower NADW is located considerably offshore of these two shallower cores and resides primarily within Region 2. Roughly a third of this flow is recirculated northward along the western side of the MAR directly beneath the middle NADW. A second cyclonic recirculation appears in the eastern basin. Southward flow is evident over the eastern side of the MAR while the remainder of the eastern basin is dominated by a relatively large net northward flow.

Schematic circulation patterns for the lower NADW are shown in Figure 13c. The western basin is dominated by a 5 Sv cyclonic recirculation cell which extends as far south as the Ceara Rise, and perhaps as far north as 15°N (Molinari et al. 1992), or even 30°N (McCartney 1992b). Associated with this recirculation is a net throughflow of -7 Sv which presumably crosses the equator as part of the DWBC. The sections of Molinari et al. carried out between 0 and 14.5°N gave an average transport of -13.0 ± 2.7 Sv within this temperature class of the DWBC. This estimate agrees well with the -12 Sv of lower NADW we find flowing across the 11°N section. In a recent study by Speer and McCartney (1992), the lower NADW, defined as all flow between 2900 and 4400 m, was found to transport -8.4 Sv of lower NADW along the western boundary across 13°N, and -13.2 Sv across 7°N - 10°N. Applying this definition to our data, we find that -10.5 Sv is flowing across our section, in good agreement with the estimates of Speer and McCartney (1992).

A second recirculation gyre of lower NADW occurs within the eastern basin. This cell is considerably greater in magnitude (6 Sv) than that of the middle NADW (1 Sv) illustrated in Figure 13b. McCartney (pers. comm.) has found that there may be a small amount of lower NADW (0.5 - 1 Sv) flowing eastward through the Vema Fracture Zone. Warren and Speer (1991) found 1.8 Sv flowing northward across 11°S within the eastern basin between 2400 and 4000 db. Although this pressure interval corresponds roughly to 2.0° - 2.7°C and thus contains most of the lower NADW as well as some of the middle

NADW, it is reasonable to assume that at least 1 Sv of lower NADW is flowing into the tropical North Atlantic via the Kane Gap. These two flows through the Vema and the Kane Gap may become entrained into the recirculation gyre and ultimately yield a 2 Sv net northward throughflow of lower NADW. Partly as a result of the surrounding topography, this current is intensified against the eastern flank of the MAR. Evidence of this flow again can be seen in the nutrient data of the recent subtropical Atlantic sections (Roemmich and Wunsch 1985) discussed above.

Beneath the lower NADW resides the AABW. As shown in Figure 10, a net AABW transport of 2.1 Sv is found crossing our 11°N section. This result agrees well with earlier results of Wright (1969), who by means of a box model found 1.4 Sv of AABW crossing 16°N, and Wright (1970), who using IGY data found 2.7 Sv of AABW crossing 8°N. Our transport of AABW is slightly smaller than more recent estimates of bottom water flow within the tropical North Atlantic. For instance, McCartney (1992a) calculated the transport of $\theta < 1.9^{\circ}\text{C}$ water across 13°N to be 3.5 - 4.5 Sv. McCartney (1992a) calculated the transport of $\theta < 1.9^{\circ}\text{C}$ across 4°N in the western basin to be between 2.7 and 4.3 Sv, depending on the method used for bottom triangle extrapolation.

Transport of AABW integrated seaward from the western boundary is shown in Figure 12h. Here we see that although there is a significant recirculation of AABW within the western basin, almost all of the net 2.1 Sv of AABW flows across the *eastern* basin. This is somewhat counterintuitive, since the Walvis Ridge at 30°S blocks northward flow of AABW within the eastern basin. Although within the South Atlantic the AABW is forced to flow northward almost entirely within the western basin, this water may enter the eastern basin of the tropical North Atlantic by means of deep fracture zones in the MAR. Two particular locations where AABW may flow through the MAR are at the Romanche Fracture Zone on the equator (Warren and Speer 1991), or at the Vema Fracture Zone just south of our section (McCartney et al. 1991). Transport results from our section indicate that nearly all of the northward flowing AABW may flow through these fracture zones in the MAR, resulting in a significant flow of AABW within the eastern basin and a negligible net transport in the western basin. However, it must be realized that this insignificant net flow of AABW in the west is partially an artifact of our definition of AABW. For instance, if we had defined the AABW to include all water with $\theta < 1.7^{\circ}\text{C}$, we would have found a net northward flow within the western basin of 1.1 Sv.

A schematic for the AABW circulation appears in Figure 13d. A 3 Sv recirculation gyre is illustrated in the western basin with a possible throughflow, as indicated by the

results of this study, of less than 1 Sv. The 2 Sv flow of AABW through the Vema Fracture Zone and the 1 Sv cyclonic recirculation cell within the eastern basin strongly support the results of McCartney et al. (1991). As a result of local topography, the 2 Sv net northward flow of AABW most likely enters the subtropical North Atlantic along the eastern flank of the MAR.

The most frequently studied feature of the deep North Atlantic circulation is the DWBC, and thus it merits some additional discussion. Definitions of the DWBC vary widely, depending primarily on the type of data (CTD's, current meters, or floats) used to obtain an estimate of its transport. In this study the magnitude of the DWBC is defined as the maximum southward transport of $\theta < 4.7^{\circ}\text{C}$ integrated seaward from the western boundary. As shown in Figure 14, this yields a transport of 26.5 ± 1.8 Sv for the DWBC, where the error bar includes the uncertainties in the bottom triangle transport, as well as the reference level error (again defined as the standard deviation of the results of the thirty reference level combinations). As a result of the small percentage of the total section area the DWBC occupies, the uncertainties in the Ekman and shallow NBC transports are insignificant. A number of previous DWBC transport estimates appear in Table 3. Our estimate is consistent with most of these estimates, and agrees particularly well with the more recently obtained values.

A number of authors have also hinted that within the tropical North Atlantic a large portion of this DWBC may be recirculated (McCartney 1992b; Johns et al. 1992a; Molinari et al. 1992), as it has been observed to do farther north in the mid-latitudes. Results from this analysis, as shown in Figure 14, confirm the existence of such a recirculation, and furthermore yield an estimate of 12.4 Sv for the northward return flow over the western flank of the MAR.

b. Meridional transports

The horizontal circulation patterns resulting from the analysis techniques described in Section 2 were shown above to be consistent with almost all recent current meter, float, and CTD data from the tropical North Atlantic. In this section, however, we will see that the net volume and heat fluxes crossing 11°N are significantly smaller than many previous estimates, while the freshwater flux is slightly larger. In the remainder of this section each of these fluxes will be computed and briefly compared with other estimates. Section 4 contains a discussion of the possible causes for the discrepancies in these net meridional fluxes.

1) VOLUME TRANSPORT

Within the Atlantic a meridional overturning cell is known to exist, where warm surface waters flow northward and cold deep waters flow southward. As defined here, this cell is composed of the NADW and AABW transports ($\theta < 4.7^\circ\text{C}$), or equivalently the AAIW, lower thermocline, thermocline, and surface water transports ($\theta > 4.7^\circ\text{C}$). The meridional overturning cell for this section is 5.2 ± 1.6 Sv, as shown in Figure 10. A comparison of this result with estimates from a number of other studies appears in Table 4. Although our result supports some of the recent modelling estimates listed here, it is only a third the size of many of the results obtained directly from hydrographic IGY data. Possible explanations for the differences in these results are discussed in Section 4.

2) HEAT TRANSPORT

Total heat transport across the 11°N section, H_{11} , can be expressed as the sum of three components:

$$H_{11} = H_e + H_w + H_g, \quad (1)$$

where H_w is the net heat transport (geostrophic plus Ekman) between the Brazil coast and the first CTD station, and H_e and H_g are the Ekman and geostrophic heat transports across the rest of the 11°N section. These heat transport components must be defined relative to a specific temperature. Since we allow no net meridional mass transport across the section, the total heat transport, H_{11} , will be independent of this reference temperature. As discussed by Bryden et al. (1991), however, the relative sizes of the components do depend on their specific definitions. Unless otherwise indicated, the components of H_{11} will be defined relative to the area averaged mean temperature of the section: $\bar{\theta} = 4.38^\circ\text{C}$.

The Ekman heat transport component is approximated as:

$$H_e = \int \int \rho C_p (\theta_e - \bar{\theta}) v_e dx dz \approx \rho C_p (\bar{\theta}_e - \bar{\theta}) M_e,$$

where ρ is the density of seawater, C_p is the specific heat capacity of seawater at constant pressure, θ_e is the potential temperature within the Ekman layer, v_e is the Ekman velocity, and M_e is the Ekman transport. (An overbar denotes a mean value.) As described in Section 2b, Ekman transport across the 11°N section is estimated to be 9.1 ± 1.8 Sv with a

mean penetration depth of roughly 100 m (Chereskin and Roemmich 1991). If we assume the Ekman velocity decreases linearly with depth, then we may reasonably estimate the mean potential temperature of the Ekman layer as a weighted average of the temperatures at the top and bottom of this layer (e.g. Hall and Bryden 1982):

$$\bar{\theta}_e = \frac{2\theta_e(z=0 \text{ m}) + \theta_e(z=100 \text{ m})}{3}. \quad (2)$$

Thus the Ekman heat transport component across the 11°N section is summarized as a northward transport of 9.1 Sv at an average temperature of 22.1 °C:

$$\begin{aligned} H_e &= (4.09 \times 10^6 \text{ J cm}^{-3} \text{ }^\circ\text{C}^{-1}) \cdot (22.1 \pm 0.3 \text{ }^\circ\text{C} - 4.38 \text{ }^\circ\text{C}) \cdot (9.1 \pm 1.8 \times 10^6 \text{ m}^3 \text{ s}^{-1}) \\ &= 6.6 \pm 1.3 \times 10^{14} \text{ W}. \end{aligned}$$

The heat transport over the western continental shelf can be approximated as:

$$H_w = \int_{60\text{m}}^{0\text{m}} \int_{100\text{km}}^{0\text{km}} \rho C_p (\theta_w - \bar{\theta}) v_w dx dz \approx \rho C_p (\bar{\theta}_w - \bar{\theta}) M_w.$$

The mass transport over the shelf, M_w , was computed from the ADCP data to be 4.5 ± 1.0 Sv, as described in Section 2b. Since no temperature data was taken along with the ADCP velocities on the continental shelf, temperatures from the first CTD station were used to estimate the average temperature of this transport to be 26.5 ± 1.5 °C. Although the error on this temperature estimate is large, it is nearly negligible in the following calculation, i.e. the error of H_w is dominated by the uncertainty in the transport value, not in the temperature value. The shallow NBC heat flux component is thus composed of a transport of 4.5 Sv at an average temperature of 26.5 °C, or:

$$\begin{aligned} H_w &= (4.09 \times 10^6 \text{ J cm}^{-3} \text{ }^\circ\text{C}^{-1}) \cdot (26.5 \pm 1.5 \text{ }^\circ\text{C} - 4.38 \text{ }^\circ\text{C}) \cdot (4.5 \pm 1.0 \times 10^6 \text{ m}^3 \text{ s}^{-1}) \\ &= 4.1 \pm 0.9 \times 10^{14} \text{ W}. \end{aligned}$$

Geostrophic heat transport is given by:

$$H_g = \int \int \rho C_p (\theta - \bar{\theta}) v dx dz.$$

Velocity can be broken down into two components, $v = v_g + v_o$, where v_g is geostrophic velocity assuming the reference level is a level of no motion, and v_o is the uniform velocity

added to the section to conserve mass, i.e. the 'true' velocity at the reference level. The above integral can thus be rewritten as:

$$H_g = \int \int \rho C_p (\theta - \bar{\theta}) v_g dx dz + \rho C_p (\bar{\theta} - \bar{\theta}) A v_o,$$

where A represents the area of the 11°N section. Because H_g is defined relative to the section averaged temperature, $\bar{\theta}$, the term representing heat transport due to the uniform velocity v_o is identically zero. The term containing v_g is integrated over all CTD pairs in the 11°N section for each of the reference level combinations described in Table 2. The mean result is a geostrophic transport of -13.6 Sv at an average temperature of 19.5 °C, or $H_g = -8.4 \pm 0.1 \times 10^{14}$ W. The error bar represents the standard deviation of the thirty estimates.

Summing the three components H_e , H_w and H_g , yields a total heat transport across 11°N of $H_{11} = 2.3 \pm 1.6 \times 10^{14}$ W. Since the heat flux in the Atlantic is so closely correlated with the meridional overturning, it is not surprising that this heat transport estimate is also rather low. As shown in Table 5, our value is considerably smaller than a number of previous tropical North Atlantic heat flux estimates. Unfortunately, since most of the studies listed in Table 5 do not provide error bars for their heat flux values, it is difficult to determine whether our estimate is consistent with any of these estimates. Further discussion of the discrepancy in these results is postponed to Section 4.

3) FRESHWATER TRANSPORT

Freshwater transport, defined as the component of seawater flux that is pure water, can be determined by means of mass and salt conservation equations. As shown below, these equations represent the mass and salt balances for the region including both the Arctic and the Atlantic Oceans, and are illustrated schematically in Figure 15.

Mass Conservation:

$$0 = \rho M_{BS} + F + \rho M_e + \rho M_w + \rho M_g + \rho M_b \quad (3)$$

In our previous volume and heat transport calculations, the North Atlantic was treated as a closed basin with the net mass transport across 11°N assumed to be identically zero. However, the flow entering the Atlantic via the Bering Strait, M_{BS} , must be considered when balancing freshwater. Coachman and Aagaard (1988) find the magnitude of this

throughflow to be 0.8 ± 0.1 Sv. The net gain of freshwater (i.e., precipitation minus evaporation plus land runoff) integrated from the Bering Strait to 11°N in the Atlantic is denoted F and is one of the two unknowns in the above equation. The Ekman, western boundary, and geostrophic components of northward mass transport across 11°N are represented by M_e , M_w , and M_g respectively. As discussed in Section 2, M_g has been defined to exactly balance the sum of M_e and M_w :

$$M_g = \int \int (v_g + v_o) dx dz = -(M_e + M_w)$$

To allow for the possibility that the net transport across the section is not identically zero (i.e., M_{BS} need not balance F exactly) a small unknown barotropic component of mass transport across 11°N , M_b , has been included in the above equation. This is equivalent to acknowledging that the small evaporative mass fluxes that were negligible in the previous heat and volume transport calculations are now an important component of the freshwater transport. Our neglect of M_b until now can be justified a posteriori by examining the magnitude of this term. Since the value of ρ does not vary substantially from one, it will be omitted in the remaining calculations.

Salt Conservation:

$$0 = M_{BS} \overline{S}_{BS} + M_e \overline{S}_e + M_w \overline{S}_w + M_b \overline{S} + M_g \overline{S}_g \quad (4)$$

Long-term measurements indicate that the transport averaged salinity of the Bering Strait throughflow, \overline{S}_{BS} , is 32.5 psu (Coachman and Aagaard 1988). The Ekman and western boundary salinities, $\overline{S}_e = 36.00 \pm 0.05$ and $\overline{S}_w = 36.20 \pm .05$ are computed by transport weighted averages, in the same manner as $\overline{\theta}_e$ and $\overline{\theta}_w$ were determined in the previous section. (See equation (2).) The area averaged salinity for the 11°N section is denoted by $\overline{S} = 34.95$ psu, while the transport averaged salinity is defined by:

$$\overline{S}_g = \frac{\int \int v S dx dz}{M_g} = 36.37 \pm 0.02 \text{ psu.}$$

Combining Equations (3) and (4) and solving for F , yields:

$$\begin{aligned}
 F &= \frac{1}{\bar{S}} \left[M_e(\bar{S}_e - \bar{S}) + M_w(\bar{S}_w - \bar{S}) + M_g(\bar{S}_g - \bar{S}) + M_{BS}(\bar{S}_{BS} - \bar{S}) \right] \\
 &= \frac{1}{34.95} \left[(9.1)(36.0 - 34.95) + (4.5)(36.2 - 34.95) \right. \\
 &\quad \left. + (-13.6)(36.37 - 34.95) + (0.8)(32.5 - 34.95) \right] \text{ Sv} \\
 &= -0.17 \text{ Sv}
 \end{aligned}$$

The sign of this result indicates that within this region, including both the North Atlantic and Arctic Oceans, net evaporation exceeds precipitation and land runoff.

The quantity we wish to determine is the freshwater transport crossing 11°N, i.e. F_{11} . This can be expressed in terms of the net gain of freshwater integrated between the Bering Strait and 11°N, F , and the freshwater transport through the Bering Strait, F_{BS} . Above we determined that $F = -0.17 \text{ Sv}$, while F_{BS} is simply given by:

$$F_{BS} = M_{BS} \left(1 - \frac{\bar{S}_{BS}}{1000} \right).$$

By definition these three quantities must sum to zero:

$$0 = F_{11} + F + F_{BS} \quad (5)$$

and thus the freshwater transport across 11°N can now be computed as follows:

$$\begin{aligned}
 F_{11} &= - (0.8) \left(1 - \frac{32.5}{1000} \right) - (-0.17) \\
 &= -0.60 \pm 0.15 \text{ Sv}.
 \end{aligned}$$

Since the flow of freshwater from the Pacific into the Arctic/Atlantic system is greater than the freshwater leaving the system (via net evaporation), the net freshwater flow across 11°N is southward.

Freshwater fluxes have been indirectly computed using North Atlantic values of air-sea freshwater exchange and land runoff. Wijffels et al. (1992) integrate these data, presented both by Baumgartner and Reichel (1975, Table 35) and more recently by Schmitt et al. (1989), southward from 65°N. As a northern boundary value they use the sum of the

freshwater transport of the Bering Strait and the precipitation and runoff over the Arctic Ocean. Results of this analysis appear in Figure 16. Our freshwater transport value of -0.60 Sv is slightly larger in magnitude than the values obtained by means of these integrations.

4. Discussion

The horizontal circulation results of this study agree very well with results of previous float, CTD, and current meter studies (e.g. Table 3) and give support to the application of our analysis techniques. However, partially as a result of the weak meridional overturning cell we find crossing our section (Table 4), the northward heat flux calculated above is considerably smaller than the indirectly computed estimates and model results shown in Table 5, and our freshwater transport of -0.60 Sv is larger in magnitude than the indirect estimates of Figure 16. A number of possible explanations for the differences in these results are discussed below.

a. Methodology

The methods used to obtain the various meridional overturning estimates shown in Table 4 vary widely. In fact, even some of the methods involving hydrographic data use different analysis techniques. Although some of the direct estimates were obtained via inversions, others were based on more traditional methods. Evidence of the differences in results caused by applying these various methods to hydrographic data was found by Roemmich and Wunsch (1985). Using a traditional reference level calculation, they found 13.7 Sv of deep water flowing southward across 36°N . When an inverse calculation was performed on the same data, 17.1 Sv of deep water was found flowing southward -- a difference of nearly 3.5 Sv.

Another possibility is that something inherent in the methodology of this analysis is causing the discrepancy in these net meridional flux estimates. For instance, what if instead of balancing mass by the addition of a uniform v_0 , mass conservation was imposed as a constraint on the system? This alternative was also tested. Even if mass conservation (without the addition of a barotropic velocity) was only supplemented by the mild constraints that the net AABW flow must be northward and the net NADW flow must be southward, the maximum possible meridional overturning cell is still only 6 Sv, and is considerably smaller than all other estimates in Table 4.

One unconventional aspect of this analysis was the division of the section into 4 separate regions. As was evident from Figures 3 and 5, a single reference level for the entire section could not produce adequate transport results. However, what if the section was divided into six regions instead of four? In order to address this question, the eastern basin, which was formerly considered as a whole, was divided into three separate regions. While western basin reference levels were kept the same as in the above analysis, all reference levels in each of the three regions of the eastern basin were examined between 1000 db and 4500 db, by 500 db increments. Since two more unknowns were added to the system, two additional constraints were also imposed: (a) the net AABW transport across the eastern basin must be between 0 and 4 Sv northward (McCartney et al. 1991), and (b) the lower NADW must be between 2 and 6 Sv (McCartney et al. 1991; Warren and Speer 1991). It was found that when these constraints are satisfied, the maximum possible meridional overturning cell is only 7 Sv, which is still considerably lower than the results directly obtained by means of IGY hydrographic data (see Table 4). Although the realm of possible reference level choices has not yet been exhausted (an inversion is clearly necessary), it does appear that the relatively low net meridional volume and heat fluxes obtained here are *not* artifacts of the specific analysis techniques applied in this study.

b. Data resolution

The relatively poor resolution of the IGY data may be another explanation as to why the estimates based on the IGY hydrographic data are greater than most of the other estimates shown in Table 4. Although the instruments employed in the 1950's were indeed less accurate, a more serious problem is the coarse vertical and horizontal resolution of these data. Beneath 2000 m measurements were taken only every 200 - 300 m. Furthermore, at 8°N, for example, the IGY data have a mid-ocean station spacing of roughly 200 km, in contrast to the nominal 50 km spacing (10 - 25 km over steep topography) used in this study. As found by Roemmich and Wunsch (1985) such low horizontal resolution can be problematic if mesoscale features are aliased into longer wavelengths and are mistaken as gyre-scale components of the general circulation.

The effect of poor horizontal resolution on these net meridional fluxes can be examined by subsampling our 11°N dataset in order to obtain station spacing similar to that of the IGY data. Subsampling in this manner yields a meridional overturning cell of up to 10.3 Sv. (If the climatological Ekman transport had been used in place of the in situ Ekman transport, this estimate would increase to 13.5 Sv). Since this estimate is twice the

size as that found by using the increased resolution available in this study, that much of the discrepancy between our result and the other direct results listed in Table 4 may be due to the coarse resolution of the IGY data.

c. Temporal variability

Temporal variability on decadal, synoptic and seasonal time scales may also explain some of the differences between the results of this study and the other estimates given in Tables 4 and 5 and in Figure 16. Each of these possibilities will now be examined in succession.

1) DECADAL

It is not implausible that the rate of NADW production in the northern North Atlantic was significantly lower in the 1980's than it was in the 1950's. In a comparison of two 1981 sections with two similar sections from the late 1950's, Roemmich and Wunsch (1985) found a significant shift of the deep southward flow in the 1981 sections toward greater depths. Evidence of this appears in their Figure 6 (reproduced here as Figure 17). A relative minimum in the transport per unit depth profiles occurs at roughly 2600 m (2.8°C - 3.0°C) for both the 24°N and the 36°N 1981 data. These minima are not apparent in the IGY data. However, a similar but stronger minimum at roughly 2600 m is apparent in the transport per unit depth profiles (referenced to the bottom) for our 1989 section (Figure 8a). This minimum corresponds to the middle core of NADW for which we find no net flow within the western basin (Figure 12b). It appears that this relative minimum in the transport of NADW between 2.4° and 3.2°C is a feature which has become increasingly evident over the past few decades. Despite this trend, Roemmich and Wunsch (1985) found that the IGY and 1981 data gave similar zonally averaged meridional transports, and thus similar heat fluxes as well. Therefore, it is not likely that this decadal variability of the middle NADW can completely account for our relatively weak meridional overturning cell and heat flux.

2) SYNOPTIC

Temporal variability on a synoptic time scale could also produce some of the differences in the estimates of Tables 4 and 5. As discussed above, the errors in the meridional overturning cell and heat flux estimates are dominated by the uncertainty in the magnitude of the Ekman and shallow NBC transports. If the meridional overturning cell is

recalculated using the climatological Ekman transport for the month of March (13.5 Sv), instead of the weaker mean in situ estimate (9.1 Sv), the magnitude of our meridional overturning cell is increased from 5.2 Sv to 8.4 Sv. This new estimate is in slightly better agreement with the other values listed in Table 4. If the heat flux estimate is similarly adjusted to include the climatological Ekman transport, our value is increased from 2.3×10^{14} W to 5.5×10^{14} W. Thus the atypically light winds characterizing this March 1989 cruise yield a net heat transport across 11°N that is less than half of that resulting from average March winds. Although this can account for a considerable amount of the discrepancy in Table 5, a similar revision of the freshwater flux estimate adjusts this value from -0.60 Sv to -0.72 Sv. This revised freshwater flux is in even *greater* disagreement with the indirect integrated estimates of Figure 16, than was the estimate based on the unusually small Ekman transport. Thus although the low winds characterizing our 11°N section can partially account for our relatively low heat transport, they cannot account for our relatively large southward freshwater transport.

3) SEASONAL

Although temporal variability on decadal or synoptic time scales may play a role in explaining some of the differences appearing in Tables 4 and 5 and in Figure 16, it is more likely that these discrepancies are linked to the strong seasonal cycles characteristic of the tropical Atlantic circulation. The Florida Current, for instance, is known to be strongly seasonal, varying from 25 Sv in January to as much as 34 Sv in June (Niiler and Richardson 1973). This seasonal cycle may be directly linked to the seasonal cycle of the tropical Atlantic circulation, since, according to Schmitz and Richardson (1991), nearly half of the transport through the Florida Straits originates in the South Atlantic. The greatest seasonal change in Ekman transport occurs at roughly $5^\circ\text{N} - 10^\circ\text{N}$ (Isemer and Hasse 1987), with a maximum in January to March, and a minimum in August to October. The seasonal variability of the NBC is even greater and is out of phase with the Ekman transport. Recent studies of the NBC indicate that the total transport of this current may range from roughly 10 Sv in the spring, to 30 - 35 Sv in the fall (Candela et al. 1992; Johns et al. 1992b).

Given this strong seasonal variability of the tropical North Atlantic, it is not surprising that our heat and freshwater flux results for March disagree with the annual average fluxes shown in Table 5 and Figure 16. In order to obtain rough estimates of the annual average fluxes across 11°N , our geostrophic transport can be forced to balance the sum of the annual average Ekman transport (roughly 10 Sv) and the shallow NBC

transport. Since the annual average total NBC transport is roughly 20 Sv, and 7 Sv were found using the CTD data offshore of the 200 m isobath (which we assume to be seasonally independent for the purpose of this computation), the annual average shallow (< 200 m) NBC transport is taken to be 13 Sv.

Inherent in such a computation is the assumption that the baroclinic component of the mid-ocean geostrophic velocity field is seasonally independent. Although this assumption has yielded reasonable net meridional fluxes in a number of previous studies (Hall and Bryden 1982; Roemmich and Wunsch 1985; Rintoul 1991; Bryden 1991), this may not be an adequate assumption in the tropical Atlantic. Some studies have shown that in this region the increasing strength of the NBC is associated with an offshore increase in the southeastward flowing North Equatorial Countercurrent (NECC) (Richardson and Walsh 1986), resulting in a constant net flow for the combined NBC and NECC system. (See Figure 18 for a schematic of equatorial currents.) Although we have adjusted the shallow NBC transport accordingly, we have not accounted for the possible increase in the southeastward flowing NECC. As a result, the annual average heat and volume fluxes presented below could be overestimates.

These calculations yield an annual average meridional overturning cell of 12 Sv. This value is in much better agreement with those listed in Table 4, and especially agrees well with the estimate of Schmitz and Richardson (1991). Although our annual estimate is still lower than most of the IGY results, it is closer to the results of two IGY sections, i.e. Rintoul (1991) at 32°S, and Roemmich and Wunsch (1985) at 36°N. The annual average geostrophic transports resulting from these assumptions (shown in Figure 19) include small northward transports of AAIW and AABW, and a relatively large southward transport of NADW. These 'reasonable' transports support the assumptions required to obtain these annual estimates, and furthermore illustrate that seasonal variability in the Ekman and shallow NBC transports may play a large role in governing the strength of the meridional overturning cell within the tropical North Atlantic.

In order to estimate annual averages heat and freshwater fluxes, transport-averaged temperatures and salinities must be attributed to the Ekman and shallow NBC transports. The annual average surface temperature is roughly 1° warmer than the average March value (Isemer and Hasse 1987), and the annual average surface salinity value is typically 1‰ fresher than the March value (Duing et al. 1980). After adjusting our previous transport averaged Ekman and shallow NBC temperatures and salinities accordingly, the annual average heat and freshwater fluxes become roughly 11×10^{14} W and -0.35 Sv,

respectively. These revised estimates can be interpreted physically as follows. Since the annual average shallow NBC transport is almost three times as strong as the March value, we would expect the annual average heat transport value also to be considerably larger than the corresponding March value ($2.3 \pm 1.6 \times 10^{14}$ W). Furthermore, within the North Atlantic March is typically a month of lower than average evaporation and higher than average precipitation (Isemer and Hasse 1987). Thus it is not surprising that our annual average freshwater flux estimate represents a somewhat smaller southward freshwater transport than the corresponding March estimate (-0.60 ± 0.15 Sv). Since the annual average estimates found above are in good agreement with previous annual average heat fluxes (Table 5) and freshwater fluxes (Figure 16), it appears that the relatively low heat and slightly high southward freshwater fluxes obtained from this March 1989 data are primarily a result of the strong seasonal variability of the tropical North Atlantic.

Although Table 5 includes only annual average heat fluxes, some seasonal estimates do exist. (As far as the author is aware, there have been no seasonal estimates of the freshwater flux in the tropical North Atlantic.) Of the previously calculated seasonal heat flux estimates for the tropical North Atlantic, only one has been obtained directly. Using IGY data from the month of May, Roemmich (1983) directly calculated the heat flux across 8°N to be 16×10^{14} W. There are a number of possible explanations for why his value is considerably larger than our 2.3×10^{14} W estimate. (1) Roemmich obtained his data from a section carried out in May while our section was performed in early March. (2) Whereas our 11°N section was characterized by weak winds, those during the 8°N IGY section may have been stronger than average. (3) The relatively poor resolution of the IGY data may also partially explain this discrepancy, and (4) the data used in Roemmich's analysis was collected more than 40 years before our 11°N transect took place. It is certainly possible that the tropical North Atlantic circulation and heat flux have changed over this extended period of time.

Estimates of the seasonal heat flux across 11°N have also been obtained indirectly by means of surface heat budget (and heat storage) analyses and by numerical models. Some of these estimates appear in Table 6. Although the surface heat budget and modelling studies can reproduce the annual average heat fluxes within the tropical North Atlantic quite well (Table 5), these studies do not produce consistent seasonal heat flux estimates. For instance, at 11°N the study of Russell et al. (1985) indicates a maximum heat transport of 24×10^{14} W between April and June, and a minimum of 4×10^{14} W between October and December. The results of Hsiung et al. (1989) show the maximum occurring earlier

(March) and the minimum occurring later (January) with magnitudes of 16×10^{14} W and -2×10^{14} W, respectively. These results contrast strongly with those of Sarmiento (1986) and of Philander and Pacanowski (1986), who both find the minimum occurring in August, and the maximum in January (precisely coinciding with Hsiung et al.'s minimum!)

As indicated by the mixed model results described above, the seasonal variability of the heat flux within the tropical North Atlantic is extremely difficult to model. As a result, it is not surprising that our direct estimate does not agree well with the numerical results. In fact, most of the models listed in Table 6 predict a larger heat flux in the spring than in the fall. If our speculation on the annual average is correct, our analysis would imply just the opposite, i.e. a greater heat transport in the fall than in the spring. The indirect results of Table 6 appear to contradict recent measurements of the NBC that show a maximum northward flow in fall, and a minimum in spring. However, as discussed above, the maximum northwestward transport of the NBC may be concurrent with the maximum southeastward transport of the NECC. Thus it is not clear whether the net flow of the combined NBC and NECC system (i.e. the Guiana Current, as shown in Figure 18) is at a maximum in the fall or in the spring, or perhaps remains roughly constant all year round (Csanady 1985). Although seasonal variability plays a potentially large role in the heat and freshwater fluxes of the tropical Atlantic, our low heat and high freshwater flux estimates indicate that this role is not yet clearly defined.

Although a number of previous studies yield annual average meridional fluxes in good agreement with those obtained above, existing seasonal heat flux values for the month of March are considerably higher than the direct estimate obtained in this study. Since heat and freshwater fluxes are highly sensitive to the NBC and Ekman transports, previous studies may have under or over estimated the seasonal variability in these transports, and thus obtained inaccurate seasonal heat flux estimates. Although indirect and modelling studies appear to be able to reproduce consistent annual estimates, we conclude that the seasonal variation of the tropical Atlantic is not yet fully understood, and is thus particularly difficult to model. This is primarily due to the paucity of observational data for the tropical Atlantic. Although there is enough data for the models to produce relatively consistent annual estimates, there is not yet enough for them to be able to obtain reliable seasonal estimates.

5. Summary

A transatlantic CTD/ADCP section nominally located at 11°N was carried out in March 1989. Relative geostrophic velocities were computed from these data via the thermal wind balance with reference level choices based primarily on water mass distributions. Mass was balanced by requiring the geostrophic transport to balance the sum of the Ekman and shallow NBC transports, as calculated from in situ wind and ADCP data.

The water column was divided into four shallow water masses (surface, thermocline, lower thermocline, and AAIW) and four deep water masses (upper NADW, middle NADW, lower NADW, and AABW). Although emphasis was placed on the circulation patterns of the deep water masses, a brief overview of the shallow water circulation was presented. The North Brazil Current (NBC) was found to flow northwestward along the western boundary with a transport of nearly 12 Sv for $\theta > 12^\circ\text{C}$. An even stronger southward counterflow (-25 Sv for $\theta > 7^\circ\text{C}$) was located just offshore of the NBC. The remainder of the section was characterized by northward flow over the western flank of the MAR, and southward flow over the eastern flank. In the eastern basin small net northward flows dominated. Transports of these water masses were found to support the results of Schmitz and Richardson (1991) who found that nearly half of the Florida Current waters are derived from the South Atlantic.

Results of the deep water analysis are summarized in the schematic circulation patterns presented in Figure 13. Within the tropical North Atlantic the west and east basins are each dominated by a cyclonic recirculation gyre. In the western basin, the upper and middle NADW cores are banked up against the western boundary, while the flow of lower NADW is farther offshore and considerably wider. The net flow of the DWBC ($\theta < 4.7^\circ\text{C}$) is found to be -26.5 ± 1.8 Sv, and agrees well with most previous estimates. Nearly half of this flow recirculates northward along the western flank of the MAR. A particularly notable result of the western basin analysis is the negligible net flow of middle NADW. Although the northward flows of upper and lower NADW along the western flank of the MAR are believed to be associated with the local recirculation gyre, the northward flow of middle NADW, which nearly balances the flow of this water mass along the western boundary, may be derived from the eastern basin of the South Atlantic.

The eastern basin is dominated by a large cyclonic recirculation gyre consisting primarily of lower NADW, and supplemented by middle NADW and AABW. Each of

these water masses, as well as the upper NADW, have small net northward flows within the eastern basin. The AABW most likely enters the eastern basin by means of the Vema Fracture Zone, while the lower NADW enters primarily through the Kane Gap. The middle and upper cores of NADW are believed to enter through both of these passages.

The components of the horizontal circulation discussed above agree well with results from previous CTD, current meter, and float studies; however, the meridional overturning cell (5.2 ± 1.6 Sv) and the net heat flux ($2.3 \pm 1.6 \times 10^{14}$ W) calculated in this study are considerably lower, and the net freshwater flux (-0.60 ± 1.5 Sv) is slightly higher than previous estimates. There are a number of possible explanations for these discrepancies. (1) *Methodology*. Most previous estimates have been obtained via numerical models or surface budgets. Even those that do directly involve hydrographic data do not necessarily use the traditional methods employed in this study, but instead are based on inversions. (2) *Resolution*. The few studies that have been obtained directly are almost exclusively based on the 1950's IGY data that have a horizontal resolution one fifth of ours, and a vertical resolution in the deep water that is orders of magnitude less than ours. (3) *Decadal variability*. Since most of the direct estimates are based on data from the 1950's, decadal variability may also play a role in explaining the above discrepancies. There is evidence that within the last 45 years the southward flowing middle core of NADW has decreased in magnitude, which could alter the magnitudes of the meridional overturning, heat, and freshwater fluxes described above. (4) *Synoptic variability*. Our section coincided with particularly weak winds. If climatological winds are used instead of the weaker in situ winds, the net volume and heat fluxes increase significantly. (5) *Seasonal variability*. Annual average meridional overturning, heat, and freshwater fluxes are computed based on annual average Ekman and NBC transports, temperatures, and salinities. The resulting values are 12 Sv, 11×10^{14} W, and -0.35 Sv respectively, which agree well with most previous annual estimates. The large difference between our March estimates and our annual estimates is indicative of the importance of seasonal variability within the tropical North Atlantic.



APPENDIX

Bottom triangles are defined as the area between the deepest common level (DCL) of a station pair and the deepest measurement of the deeper station. Within bottom triangles there is not enough information to calculate geostrophic velocities using the dynamic method. Depending on the slope of the topography and the distance between stations, neglect of bottom triangle transport can potentially induce a large error into transport calculations; this possibility must be examined. After describing various methods that have been used to attribute transport values to the bottom triangles, two different methods will be applied to this data set and the results compared.

In some instances ignoring all transport within bottom triangles may be a satisfactory solution. If the area of the bottom triangles is small as a result of closely spaced stations over relatively flat topography, and if there are no suspected bottom-intensified currents, the error due to assuming zero or constant velocity within the bottom triangles may be small. This method may be adequate for a calculation of the total transport across a section; however, significant errors may still result if the bottom or lower deep water transports are examined individually.

A slightly more sophisticated calculation of bottom triangle transport can be obtained by keeping velocity shear constant within the bottom triangle. In this manner changes in velocity can be extrapolated down into the bottom triangle. However, this method also becomes suspect if the vertical density gradient is believed to change over the range of extrapolation. A refinement of this model (Roemmich 1979; Zemba 1991) involves weighting the vertical shear by the ratio:

$$\frac{N^2(z)}{N^2(z_{dcl})} \quad (A-1)$$

where $N(z_{dcl})$ is the Brunt-Vaisala frequency at the deepest common level of the two stations, and $N(z)$ is the Brunt-Vaisala profile for the deeper station within the bottom triangle. The latter is thus determined solely from data at the deeper of the two stations. This method assumes that the separation and slope of isopycnals remains constant within the bottom triangles.

If any non-zero velocity is ascribed to the bottom triangles, the possibility of topographic blocking must be considered. Over rough topography the bottom area between

two stations frequently cannot be adequately approximated by a triangle. For instance, hills in the sea-floor bathymetry can cause bottom 'triangles' to be partially or entirely blocked. An example of such intervening topography is shown in Figure A1. Station locations are overlaid on the topography across two parts of the 11°N section: (a) along the eastern continental slope, and (b) along the western side of the Mid-Atlantic Ridge (MAR). In Figure A1a, the area below the DCL of any two stations is well represented by a triangle; however, in Figure A1b, most of the bottom triangles are at least partially occupied by topography. As can be seen from Figure 6, Figure A1b is actually more representative of the section as a whole.

An argument can sometimes be made for ignoring intervening topography. The geostrophic current may divide and accelerate around the topography, causing the calculated transport to be equal to the product of the true reduced areas and the increased velocities (McCartney 1992a). Although this may be true for some of the narrow (relative to the station spacing) spikes occurring in the bathymetry (see Figure 6), intervening topography cannot be ignored in the many bottom triangles which are *completely* occupied by topography. In this study we assume that intervening topography can be ignored everywhere except within the bottom triangles, i.e., outside the bottom triangles the topography is assumed not to support any pressure gradient. After examining each station pair individually the bottom triangle areas are adjusted to include only that area not blocked by topography.

In this study two methods of obtaining bottom triangle transport are compared. (The reference levels used to obtain these transports is discussed in Section 2c, and are shown in Table 2.) In the first method velocities within the bottom triangles are assumed to be constant and equal to the velocity at the DCL, and in the second method the vertical shear is assumed to be weighted by the ratio given in Equation (A-1). In each case bottom triangle areas are adjusted to account for topographic blocking as described above. Figure A2 shows integrated bottom triangle transport of AABW ($\theta < 1.8^\circ\text{C}$) and lower NADW ($1.8^\circ < \theta < 2.4^\circ\text{C}$) as computed by each of these methods. For both the AABW and the lower NADW, individual bottom triangle transports differ by less than 0.3 Sv, depending on the method chosen. When these transports are integrated over the entire section, the differences between these two methods are roughly 0.3 Sv for the AABW and 0.4 Sv for the lower NADW. (For all other water masses the integrated differences are less than 0.1 Sv.) For consistency, the more sophisticated weighted shear method is used for all bottom triangles with the exception of those described below.

For the four shallowest station pairs (all less than 1400 m depth), we consistently approximate the DCL of the two stations as a level of no motion. (Reference level choice is addressed in Section 2c.) In such a situation the use of the weighted vertical shear method would unrealistically attribute a bottom triangle velocity with a sign opposite to that of the velocity just above the level of no motion. (One could avoid this velocity reversal by assuming a level of no motion at the deepest point of the deeper of the two stations instead of at the DCL. However, for these particular station pairs this process gives exceptionally large velocities which are in disagreement with nearby current meter, float and ADCP data.) Since there is no evidence to suggest that a velocity reversal at depth exists, we assume no bottom triangle transport for these particular station pairs.

The weighted vertical shear method is also inappropriate for two station pairs located along the western continental slope, #81/82 and #80/81, and one station pair along the eastern continental slope, #3/4. At station pair #81/82 the velocity directly above the DCL increases strongly with depth. As illustrated in Figure A3, velocity extrapolation by means of a weighted vertical shear causes the velocities within this bottom triangle to be extremely large and positive (though admittedly smaller than if we had assumed a constant vertical shear). Even the use of the first method described above, i.e. assuming a constant velocity of 27.5 cm/s, results in an unacceptably large bottom triangle transport of 0.8 Sv. Since tracer data indicates that the southward flowing core of upper NADW is banked up against the continental slope at 1800 m, this large *positive* bottom triangle transport is disturbing. Furthermore, this core of upper NADW is evident in the velocity profile of the deeper adjacent station pair (see Figure A3), and thus again argues against a large positive bottom triangle transport at 1800 m for station pair #81/82. With no way of determining precisely how much of the upper NADW core is located within this bottom triangle, it is reasonable to assume that the northward transport roughly cancels the expected southward transport. Thus we attribute no net bottom triangle transport to this station pair. Since a similar scenario exists for station pairs #80/81 and #3/4 we assume no net transport in these bottom triangles as well.

The maximum error incurred by using the weighted shear method is assumed to be equal to the magnitude of the bottom triangle transport, while the minimum error is probably roughly equal to the difference in the results of the two methods described above and shown in Figure A2. The error in AABW transport resulting from the uncertainty in the bottom triangle flow is thus assumed to range between 0.3 and 1.8, or on average roughly 1 Sv. As a result of the relatively small net transports of AABW this uncertainty is

significant, and is the dominant source of error in all AABW transport estimates throughout this paper. The bottom triangle error associated with the lower NADW is assumed to range between 0.4 and 0.6 Sv, but as a result of the typically large transports of lower NADW, this error is typically small as compared to the errors in the Ekman and western boundary transport estimates as well as that due to reference level choice. As a result of the small bottom triangle areas associated with each of the shallower water masses, in these cases errors due to bottom triangle transport uncertainty are negligible.

REFERENCES

- Amos, A. F., A. L. Gordon, and E. D. Schneider, 1971: Water masses and circulation patterns in the region of the Blake-Bahama Outer Ridge. *Deep-Sea Res.*, **18**, 145-166.
- Barrett, J. R., 1965: Subsurface currents off Cape Hatteras. *Deep-Sea Res.*, **12**, 173-184.
- Baumgartner, A., and E. Reichel, 1975: *The World Water Balance*. Elsevier.
- Bennett, S. L., and M. S. McCartney, 1990: The Large Transport Deep Western Boundary Current and Its Recirculation in the Low Latitude Atlantic. *Eos, Trans. Amer. Geophys. Union*, **71**, 168 (abstract).
- Bryden, H. L., D. H. Roemmich, and J. A. Church, 1991: Ocean heat transport. *Deep-Sea Res.*, **38**, 297-324.
- Bunker, A. F., 1976: Computations of surface energy flux and annual air-sea interaction cycles of the North Atlantic Ocean. *Mon. Wea. Rev.*, **104**, 1122-1140.
- Candela, J., R. Limeburner, and R. Beardsley, 1992: The Flow of the North Brazil Current over the Amazon Shelf. *Eos, Trans. Amer. Geophys. Union*, **71**, 1410 (abstract).
- Chereskin, T. K., and D. Roemmich, 1991: A comparison of measured and wind-derived Ekman transport at 11°N in the Atlantic Ocean. *J. Phys. Oceanogr.*, **21**, 869-878.
- Coachman, L. K., and K. Aagaard, 1988: Transports through Bering Strait: Annual and interannual variability. *J. Geophys. Res.*, **93**, 15,535-15,539.
- Cochrane, J. D., F. J. Kelly Jr., and C. R. Olling, 1979: Subthermocline countercurrents in the western equatorial Atlantic Ocean. *J. Phys. Oceanogr.*, **9**, 724-738.
- Csanady, G. T., 1985: A zero potential vorticity model of the North Brazilian Coastal Current. *J. Mar. Res.*, **43**, 553-579.
- Duing, W., F. Ostapoff, and J. Merle, 1980: *Physical Oceanography of the Tropical Atlantic during GATE*. University of Miami.
- Fine, R. A., and R. L. Molinari, 1988: A continuous deep western boundary current between Abaco (26.5°N) and Barbados (13°N). *Deep-Sea Res.*, **35**, 1441-1450.
- Hall, M. M., and H. L. Bryden, 1982: Direct estimates and mechanisms of ocean heat transport. *Deep-Sea Res.*, **29**, 339-359.
- Hellerman, S., and M. Rosenstein, 1983: Normal monthly wind stress over the world ocean with error estimates. *J. Phys. Oceanogr.*, **32**, 1093-1104.
- Hsiung, J., 1985: Estimates of global oceanic meridional heat transport. *J. Phys. Oceanogr.*, **15**, 1405-1413.
- Hsiung, J., R. E. Newell, and T. Houghtby, 1989: The annual cycle of oceanic heat storage and oceanic meridional heat transport. *Q. J. R. Meteorol. Soc.*, **115**, 1-28.

- Isemer, H. J., and L. Hasse, 1987: *The Bunker Climate Atlas of the North Atlantic Ocean*. New York: Springer-Verlag.
- Johns, W. E., D. M. Fratantoni, and R. J. Zantopp, 1992a: Deep Western Boundary Current variability off Northeastern Brazil. *Deep Sea Res.*, accepted.
- Johns, W. E., T. N. Lee, F. A. Schott, R. J. Zantopp, and R. Evans, 1990: The North Brazil Current Retroflexion: seasonal structure and eddy variability. *J. Geophys. Res.*, **95**, 22,103-22,120.
- Johns, W. E., T. N. Lee, and R. J. Zantopp, 1992b: Seasonal Cycle and Variability of the North Brazil Current at 4°N in the Tropical Atlantic. *Eos, Trans. Amer. Geophys. Union*, **71**, 1425 (abstract).
- Lai, D. Y., 1984: Mean flow and variabilities in the deep western boundary current. *J. Phys. Oceanogr.*, **14**, 1488-1498.
- Lamb, F. J., 1981: Estimate of annual variation of Atlantic Ocean heat transport. *Nat.*, **290**, 766-768.
- Leaman, K. D., and J. E. Harris, 1990: On the average absolute transport of the Deep Western Boundary Currents East of Abaco Island, the Bahamas. *J. Phys. Oceanogr.*, **20**, 467-475.
- Lee, T. N., W. Johns, F. Schott, and R. Zantopp, 1990: Western boundary current structure and variability east of Abaco, Bahamas at 26.5°N. *J. Phys. Oceanogr.*, **20**, 446-466.
- McCartney, M. S., 1992a: The transport of Antarctic bottom water at 4°N in the western basin of the North Atlantic Ocean. *J. Geophys. Res.*, in press.
- McCartney, M. S., 1992b: The crossing of the equator by the deep western boundary current in the western Atlantic Ocean. *J. Phys. Oceanogr.*, in press.
- McCartney, M. S., and R. Curry, 1992: Trans-equatorial flow of Antarctic bottom water in the western Atlantic Ocean: abyssal geostrophy at the equator. *J. Phys. Oceanogr.*, in press.
- McCartney, M. S., S. L. Bennett, and M. E. Woodgate-Jones, 1991: Eastward flow through the Mid-Atlantic Ridge at 11°N and its influence on the abyss of the eastern basin. *J. Phys. Oceanogr.*, **21**, 1089-1121.
- Molinari, R. L., R. A. Fine, and E. Johns, 1992: The Deep Western Boundary Current in the Tropical North Atlantic Ocean. *Deep Sea Res.*, accepted.
- Niiler, P. P., and W. S. Richardson, 1973: Seasonal variability of the Florida Current. *J. Mar. Res.*, **31**, 144-167.
- Philander, S. G. H., and R. C. Pacanowski, 1986: The mass and heat budget in a model of the tropical Atlantic Ocean. *J. Geophys. Res.*, **91**, 14,212-14,220.
- Richardson, P. L., 1977: On the crossover between the Gulf Stream and western boundary undercurrent. *Deep-Sea Res.*, **24**, 139-159.

- Richardson, P. L., and J. A. Knauss, 1971: Gulf Stream and western boundary undercurrent observations at Cape Hatteras. *Deep-Sea Res.*, **18**, 1089-1109.
- Richardson, P. L., and W. J. Schmitz Jr., 1992: Deep cross-equatorial flow in the Atlantic measured with SOFAR floats. *J. Geophys. Res.*, submitted.
- Richardson, P. L., and D. Walsh, 1986: Mapping climatological seasonal variations of surface currents in the tropical Atlantic using ship drifts. *J. Geophys. Res.*, **91**, 10,537-14,550.
- Rintoul, S. R., 1991: South Atlantic interbasin exchange. *J. Geophys. Res.*, **96**, 2675-2692.
- Roemmich, D., 1979: The application of inverse methods to problems in ocean circulation. Ph.D. Thesis, MIT/WHOI, WHOI-80-6.
- Roemmich, D., 1983: The balance of geostrophic and Ekman transports in the tropical Atlantic Ocean. *J. Phys. Oceanogr.*, **13**, 1534-1539.
- Roemmich, D., and C. Wunsch, 1985: Two transatlantic sections: meridional circulation and heat flux in the subtropical North Atlantic Ocean. *Deep-Sea Res.*, **32**, 619-664.
- Russell, G. L., J. R. Miller, and L. C. Tsang, 1985: Seasonal oceanic heat transports computed from an atmospheric model. *Dyn. Atmos. Oceans*, **9**, 253-271.
- Sarmiento, J. L., 1986: On the north and tropical Atlantic heat balance. *J. Geophys. Res.*, **91**, 11,677-11,689.
- Schmitt, R. W., P. S. Bogden, and C. E. Dorman, 1989: Evaporation minus precipitation and density fluxes for the North Atlantic. *J. Phys. Oceanogr.*, **19**, 1208-1221.
- Schmitz, W. J., Jr., and M. S. McCartney, 1992: On the North Atlantic Circulation. *Rev. Geophys.*, accepted.
- Schmitz, W. J., Jr., and P. L. Richardson, 1991: On the sources of the Florida Current. *Deep-Sea Res.*, **38** (Suppl), S379-S409.
- Semtner, A. J., and R. M. Chervin, 1988: A simulation of the global ocean circulation with resolved eddies. *J. Geophys. Res.*, **93**, 15,502-15,522.
- Semtner, A. J., and R. M. Chervin, 1992: Ocean general circulation from a global eddy-resolving model. *J. Geophys. Res.*, **97**, 5493-5550.
- Speer, K. G., and M. S. McCartney, 1992: Tracing Lower North Atlantic Deep Water across the equator. *J. Geophys. Res.*, **96**, 20,443-20,448.
- Speer, K. G., and E. Tziperman, 1992: Rates of water mass formation in the North Atlantic Ocean. *J. Phys. Oceanogr.*, **22**, 93-104.
- Stommel, H., and A. B. Arons, 1960: On the abyssal circulation of the world ocean - II. An idealized model of the recirculation pattern and amplitude in oceanic basins. *Deep-Sea Res.*, **6**, 217-233.

- Swallow, J. C., and L. V. Worthington, 1961: An observation of a deep counter-current in the western North Atlantic. *Deep-Sea Res.*, **8**, 1-9.
- Tucholke, B. E., W. R. Wright, and C. D. Hollister, 1973: Abyssal circulation over the Greater Antilles Outer Ridge. *Deep-Sea Res.*, **20**, 973-995.
- Warren, B. A., and K. G. Speer, 1991: Deep circulation in the eastern South Atlantic Ocean. *Deep-Sea Res.*, **38** (Suppl), S281-S322.
- Whitehead, J. A., and L. V. Worthington, 1982: The flux and mixing rates of Antarctic Bottom water within the North Atlantic. *J. Geophys. Res.*, **87**, 7903-7924.
- Wijffels, S., H. Bryden, R. Schmitt, and A. Stigebrandt, 1992: On the transport of freshwater by the oceans. *J. Phys. Oceanogr.*, **22**, 155-162.
- Wright, W. R., 1969: Deep water movement in the western Atlantic as determined by use of a box model. *Deep-Sea Res.*, **16** (Suppl), 433-446.
- Wright, W. R., 1970: Northward transport of Antarctic Bottom Water in the western Atlantic Ocean. *Deep-Sea Res.*, **17**, 367-371.
- Wunsch, C., 1984: An eclectic Atlantic Ocean circulation model. Part I: the meridional flux of heat. *J. Phys. Oceanogr.*, **14**, 1712-1733.
- Wust, G., 1935: *The stratosphere of the Atlantic Ocean*. New Delhi, India: Amerind Publishing.
- Wust, G., 1955: Stromgeschwindigkeiten im Tiefen und Bodenwasser des Atlantischen Ozeans auf Grund dynamischer Berechnung der *Meteor* Profile der Deutschen Atlantischen Expedition 1925/27. *Deep-Sea Res.*, **3** (Suppl), 373-397.
- Wust, G., 1957: Quantitative untersuchungen zur statik und dynamik des Atlantischen Ozeans, Stromgeschwindigkeiten und strommengen in den tiefen des Atlantischen Ozeans unter besonderer berucksichtigung des tiefenund bodenwassers. *Wiss. Ergebn. dt. atlant. Exped. Meteor 1925-27*, **VI**, 261-420.
- Zemba, J. C., 1991: The Structure and Transport of the Brazil Current between 27° and 36° South. Ph.D. Thesis, MIT/WHOI, WHOI-91-37.

TABLE 1. Definitions of water masses in terms of potential temperature classes.

surface water	$\theta > 24^{\circ}\text{C}$
thermocline water	$12^{\circ} < \theta < 24^{\circ}\text{C}$
lower thermocline water	$7^{\circ} < \theta < 12^{\circ}\text{C}$
AAIW	$4.7^{\circ} < \theta < 7.0^{\circ}\text{C}$
upper NADW	$3.2^{\circ} < \theta < 4.7^{\circ}\text{C}$
middle NADW	$2.4^{\circ} < \theta < 3.2^{\circ}\text{C}$
lower NADW	$1.8^{\circ} < \theta < 2.4^{\circ}\text{C}$
AABW	$\theta < 1.8^{\circ}\text{C}$

TABLE 2. The 30 combinations of reference levels for Regions 2 and 3, selected such that the net flow of AABW within the western basin is > -0.5 Sv (before mass conservation is imposed) and total NADW transport is maximized. These combinations, also depicted in Figure 9b, are associated with a 1100 db reference level in Region 1 and a 2100 db reference level in Region 4.

Reference level for Region 2 [db]	Reference level for Region 3 [db]
2000	1600
2200	1700
2200	1800
2300	1800
2300	1900
2400	1900
2400	2000
2500	1900
2500	2000
2500	2100
2600	2000
2600	2100
2600	2200
2700	2000
2700	2100
2700	2200
2700	2300
2800	2100
2800	2200
2800	2300
2800	2400
2900	2100
2900	2200
2900	2300
2900	2400
2900	2500
3000	2200
3000	2300
3000	2400
3000	2500

TABLE 3. Estimates of the DWBC.

	Method	lat. [°N]	DWBC [Sv]
Stommel and Arons, 1960	geostrophic velocities	35°	20
Swallow and Worthington, 1961	geostrophic velocities referenced to direct velocity measurements; data below 1000m	33°	7
Barrett, 1965	geostrophic velocities referenced to direct velocity measurements; data below 150m	35°	12
Richardson & Knauss, 1971	geostrophic velocities referenced to direct velocity measurements	35°	10
Amos et al., 1971	geostrophic velocities referenced to 2000m; data below 2000m	30°	22
Richardson, 1977	geostrophic velocities referenced to direct velocity measurements; data below 1000m	35°	24
Lai, 1984	current meters; data below 800m	28°	24
Fine & Molinari, 1988	geostrophic velocities referenced to bottom; data below 1000m	26.5° 19°	23.8 8.3
Lee et al., 1990	current meters; data below 800 m	26.5°	30
Leaman and Harris, 1990	geostrophic velocities referenced to PEGASUS data; data below 800 m	26.5°	35
Molinari et al., 1992	geostrophic velocities referenced to 4.7°C; data below 4.7°C	0°- 14.5°	17.5-33.0
Johns et al., 1992a	current meter; data below 2500m	8°	22
this study	data below 4.7°	8-9°	26.5 ± 1.8

TABLE 4. Estimates of the meridional overturning cell in the Atlantic Ocean, defined as the total NADW plus AABW transport, or equivalently the net transport above (or below) roughly 4° - 5° C.

	Method	Meridional Cell [Sv]
Hall & Bryden, 1982	IGY hydrography @ 24°N October, 1957	15.6
Roemmich, 1983	IGY hydrography @ 8°N May, 1957	21
Roemmich & Wunsch, 1985	hydrography @ 24°N IGY October, 1957 / August, 1981	18 / 18 [†]
Roemmich & Wunsch, 1985	hydrography @ 36°N IGY April-May, 1957 / June, 1981	12 / 17 [†]
Sarmiento, 1986	model results at 11°N	10
Semtner & Chervin, 1988	model results at 11°N	7.5
Rintoul, 1991	IGY hydrography @ 32°S April-June, 1959	13
Schmitz and Richardson, 1991	hydrography of Florida Straits and Caribbean passages	13
Semtner & Chervin, 1992	model results at 11°N	10
Speer & Tziperman, 1992	air-sea heat and freshwater flux data	7 [*]
this study	hydrography @ 11°N March, 1989	5.2 ± 1.6

[†] Results shown are from reference level calculations using total transport constraints. First number is obtained using IGY data from 1957 while second is obtained using 1981 data.

^{*} From air-sea data a deep water sinking rate of 9 Sv is determined for the North Atlantic. Combining this with a typical AABW transport of 2 Sv yields an overturning rate of 7 Sv.

TABLE 5. Indirect and model estimates of the annual average heat transport across 10° - 11°N in the Atlantic.

	METHOD	HEAT FLUX [x 10 ¹⁴ W]
Bunker, 1976	surface heat budget	8.2
Lamb, 1981	surface heat budget	11.3
Russell et al., 1985	model	14
Hsiung, 1985	surface heat budget	8
Sarmiento, 1986	model	8
Philander & Pacanowski, 1986	model	9.5
Semtner & Chervin, 1988	model	6
Semtner & Chervin, 1992	model	8

TABLE 6. Indirect and model estimates of heat transport across 11°N in March.

	METHOD	HEAT FLUX [x 10 ¹⁴ W]
Russell et al., 1985	model	19*
Sarmiento, 1986	model	12
Philander & Pacanowski, 1986	model	14
Hsiung et al., 1989	surface heat budget	17

* this estimate represents an average over January, February, and March.

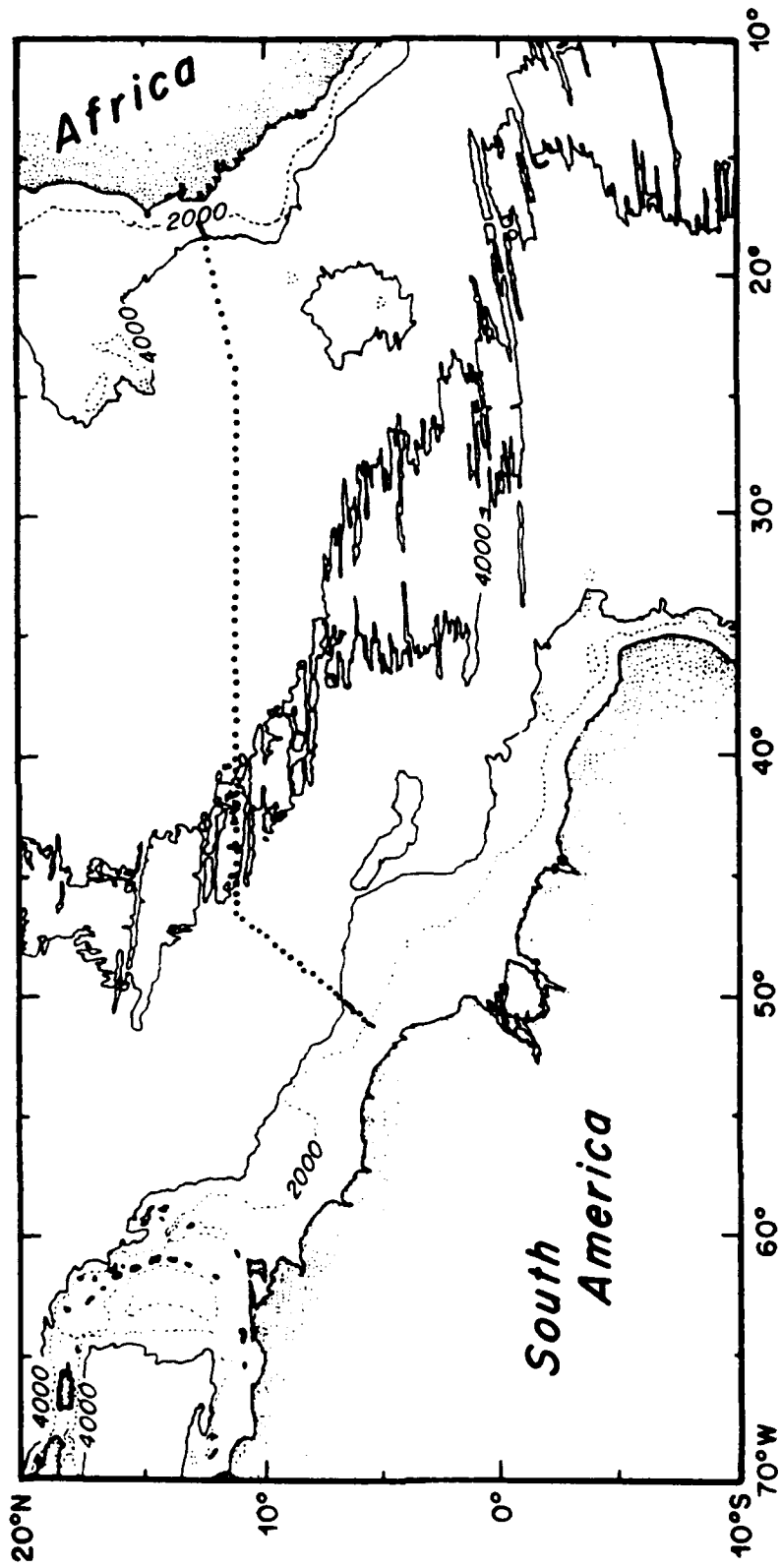


FIG. 1. Cruise track of the 11°N section in the tropical Atlantic. Individual dots denote locations of the 84 CTD's.

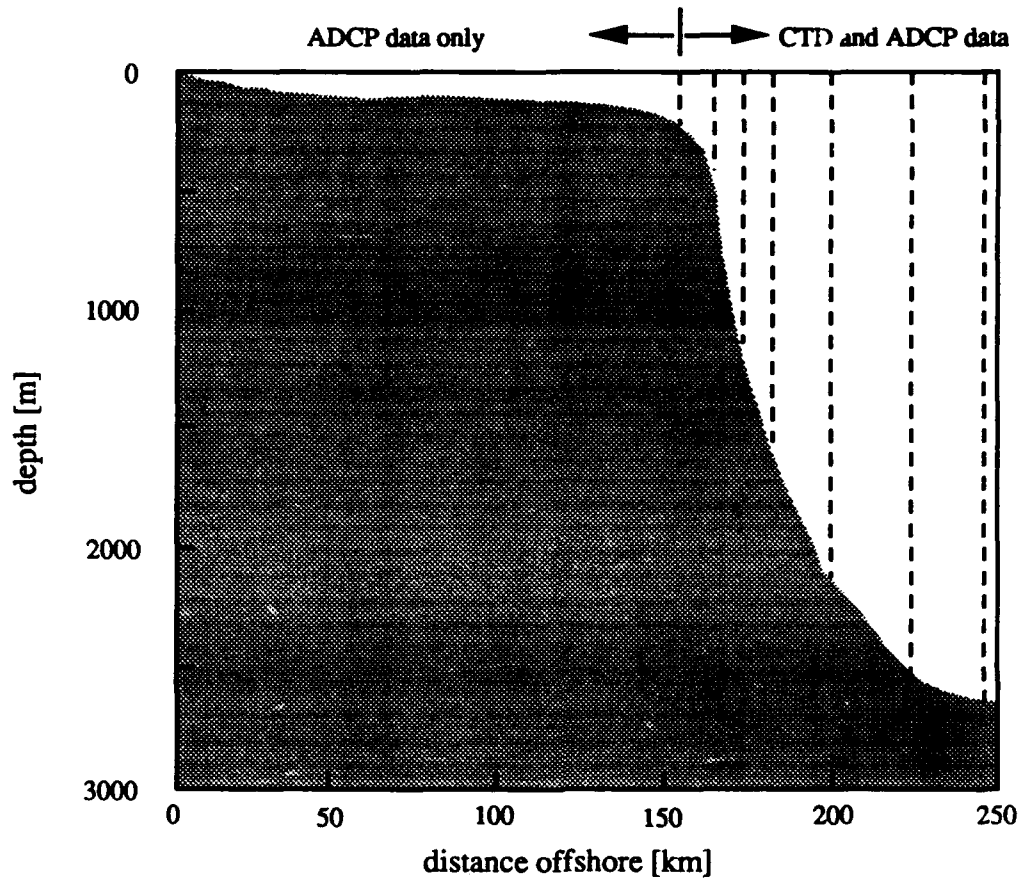


FIG. 2. Schematic of the depth profile of the westernmost 250 km of the 11°N section. The shallowest of the CTD's (depicted above by dashed lines) was taken at the 200 m isobath, roughly 150 km offshore. To the west of this CTD, only ADCP data exists.

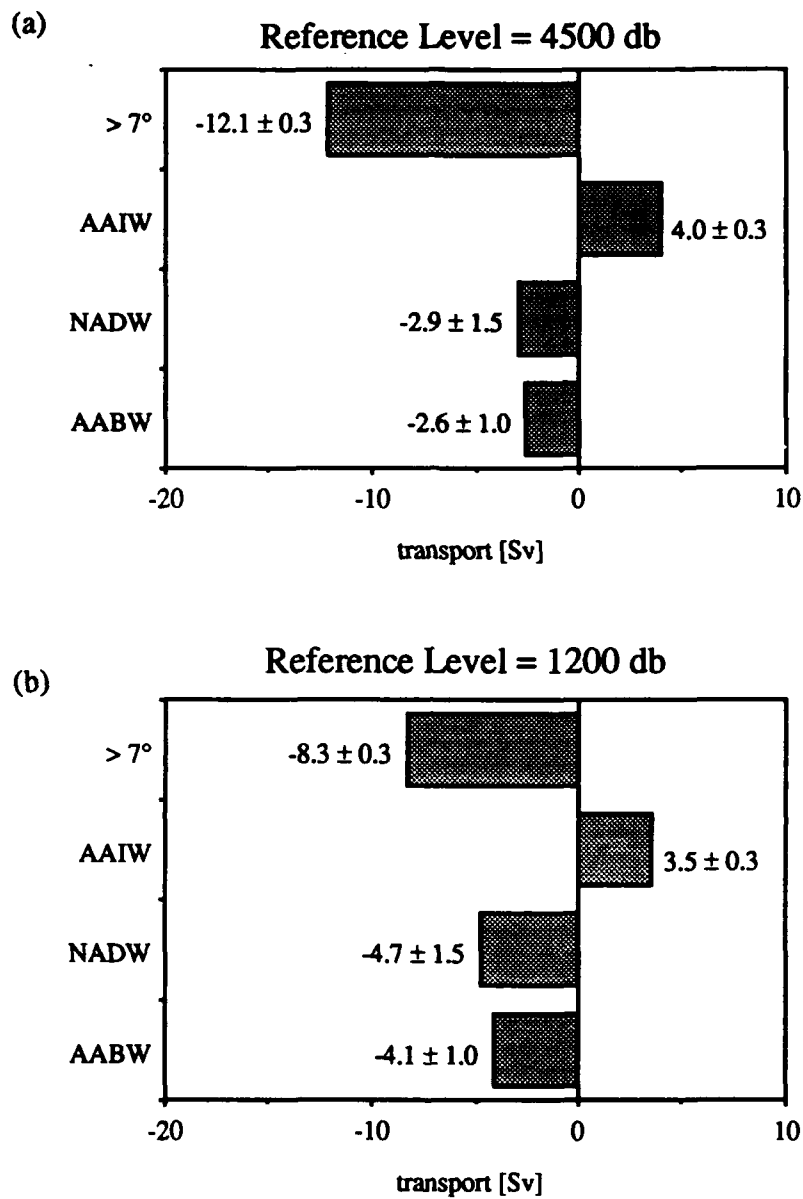


FIG. 3. Geostrophic transports in various temperature classes (as defined in Table 1) for two historical reference levels (a) 4500 db and (b) 1200 db. Net geostrophic transport is forced to be equal and opposite to the sum of the Ekman and shallow NBC transports by adding a uniform reference velocity to the section of: (a) $v_o = -0.21$ cm/s and (b) $v_o = +0.08$ cm/s.

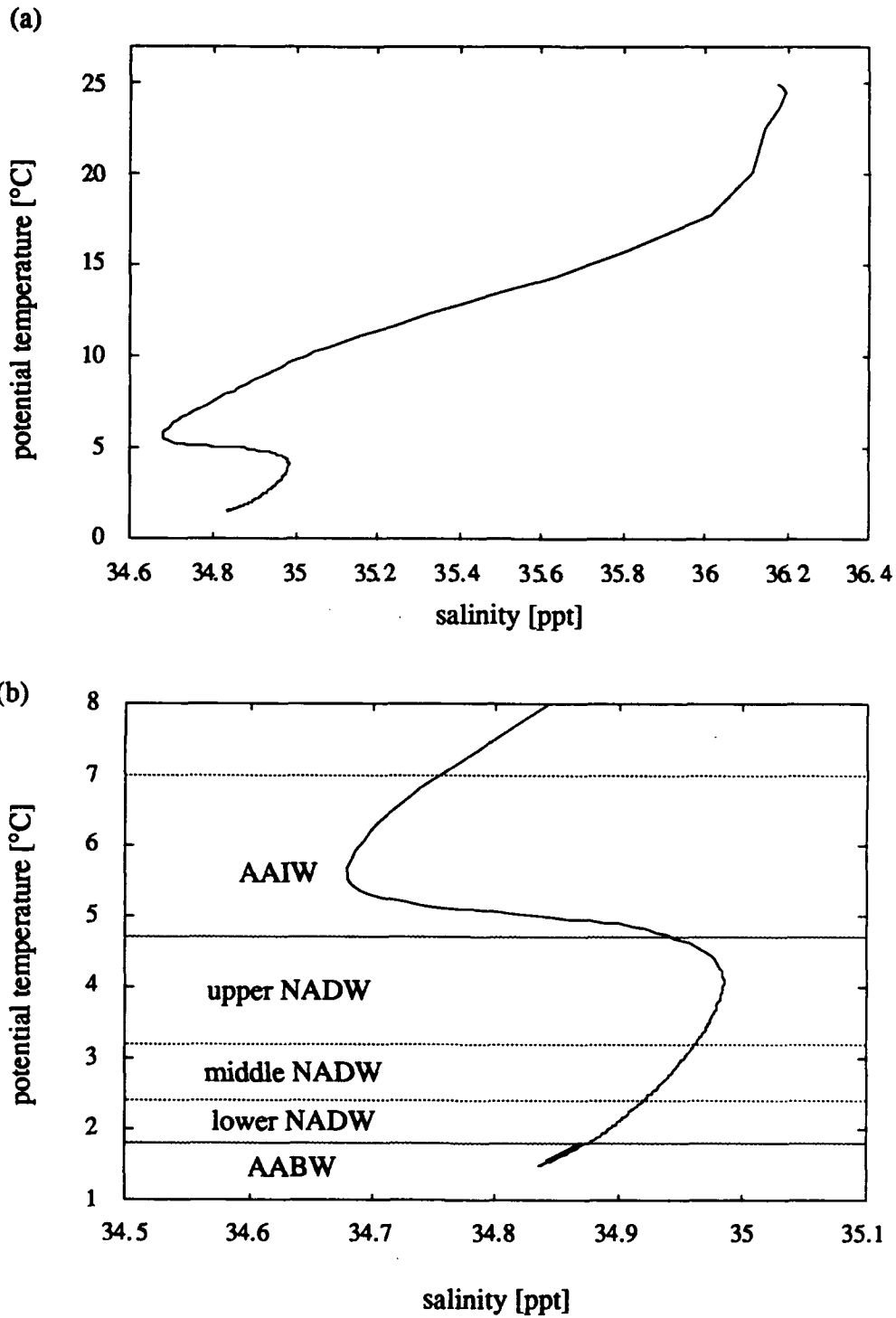


FIG. 4. A θ -S diagram for the 11°N section, calculated by taking the average potential temperature and salinity at 20 m depth intervals, for (a) the entire water column, and (b) the isothermal boundaries defining the intermediate, deep and bottom water masses.

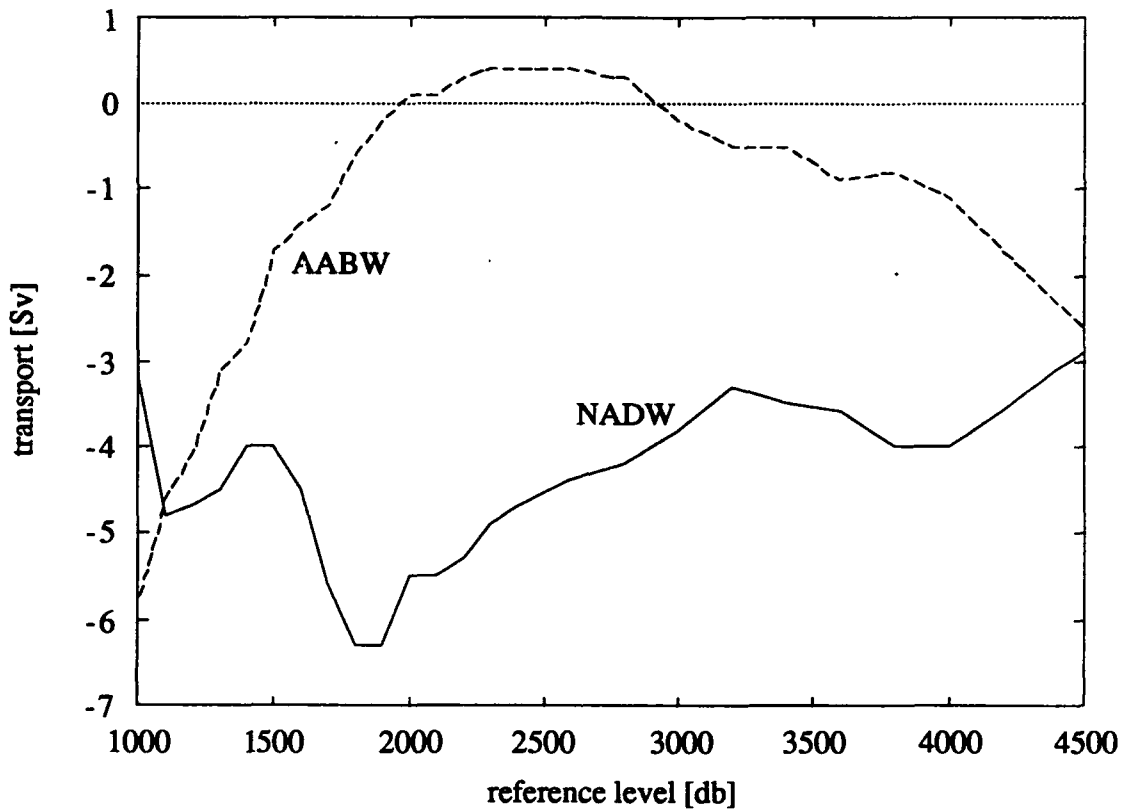


FIG. 5. Transports of AABW and NADW, as defined in Table 1, as a function of reference level for the entire 11°N section. For each reference level mass is conserved by forcing the geostrophic transport to be equal and opposite to the sum of the Ekman and shallow NADW transports.

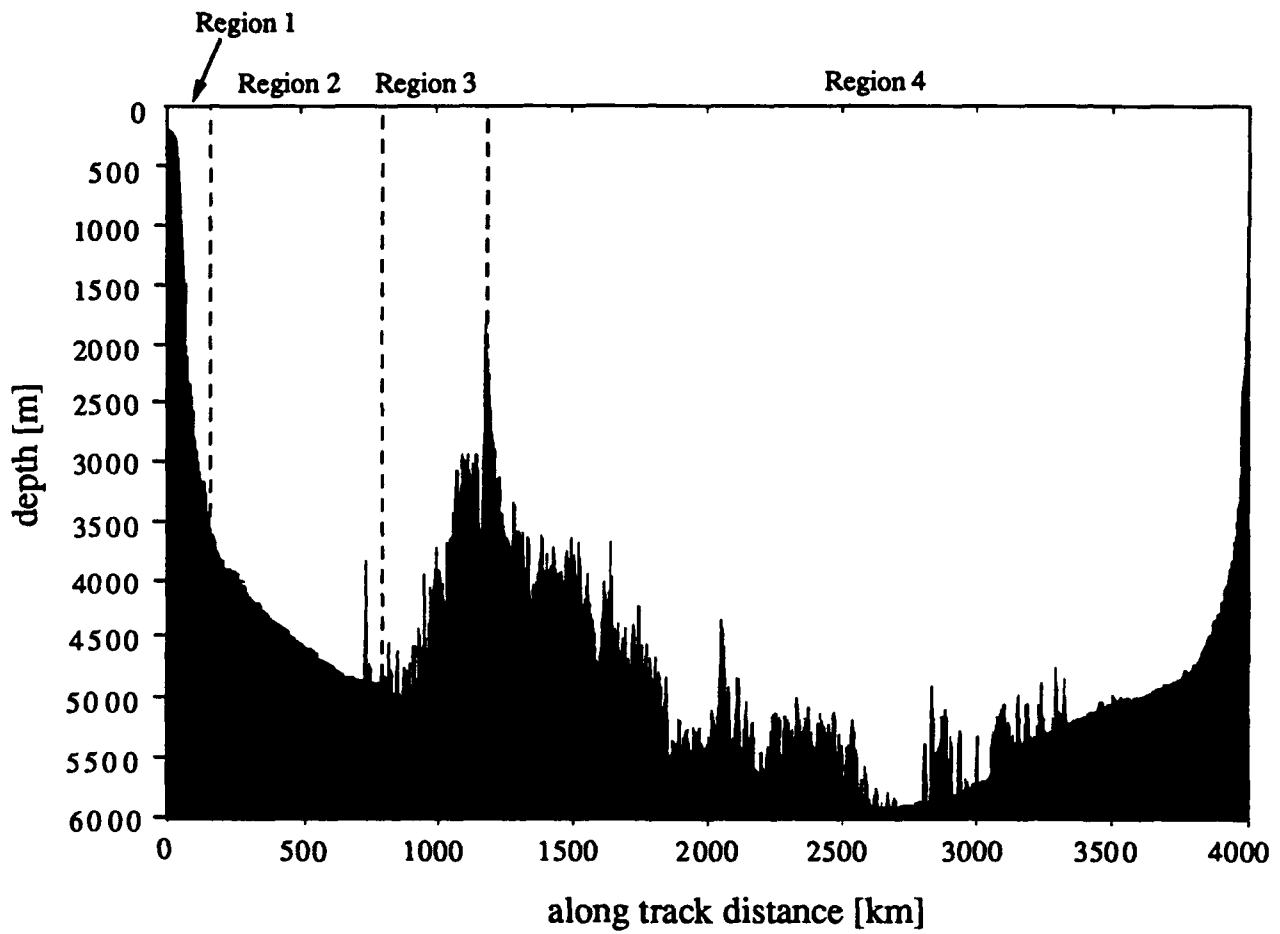


FIG. 6. Topography of the 11°N transect offshore of the shelf break. The section is divided into 4 separate regions for reference level computations, as per text.

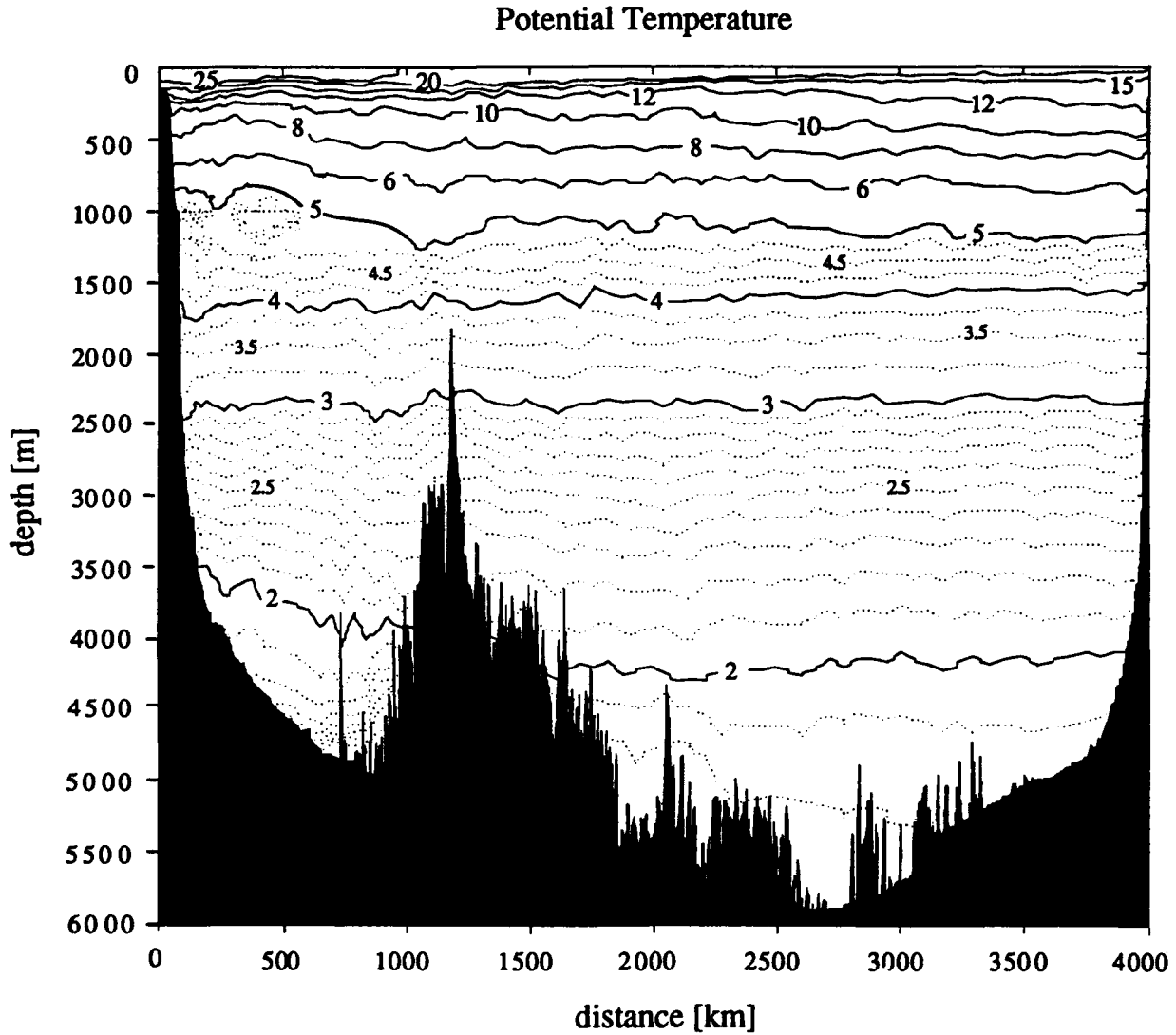


FIG. 7. Property distributions along the 11°N section from French Guiana (on the left) to Senegal, as a function of depth (m) and along track distance (km) offshore of the shelf break. (a) potential temperature (°C), (b) salinity (ppt), (c) dissolved oxygen (ml/l), (d) silicate ($\mu\text{mol/l}$), and (e) phosphate ($\mu\text{mol/l}$).

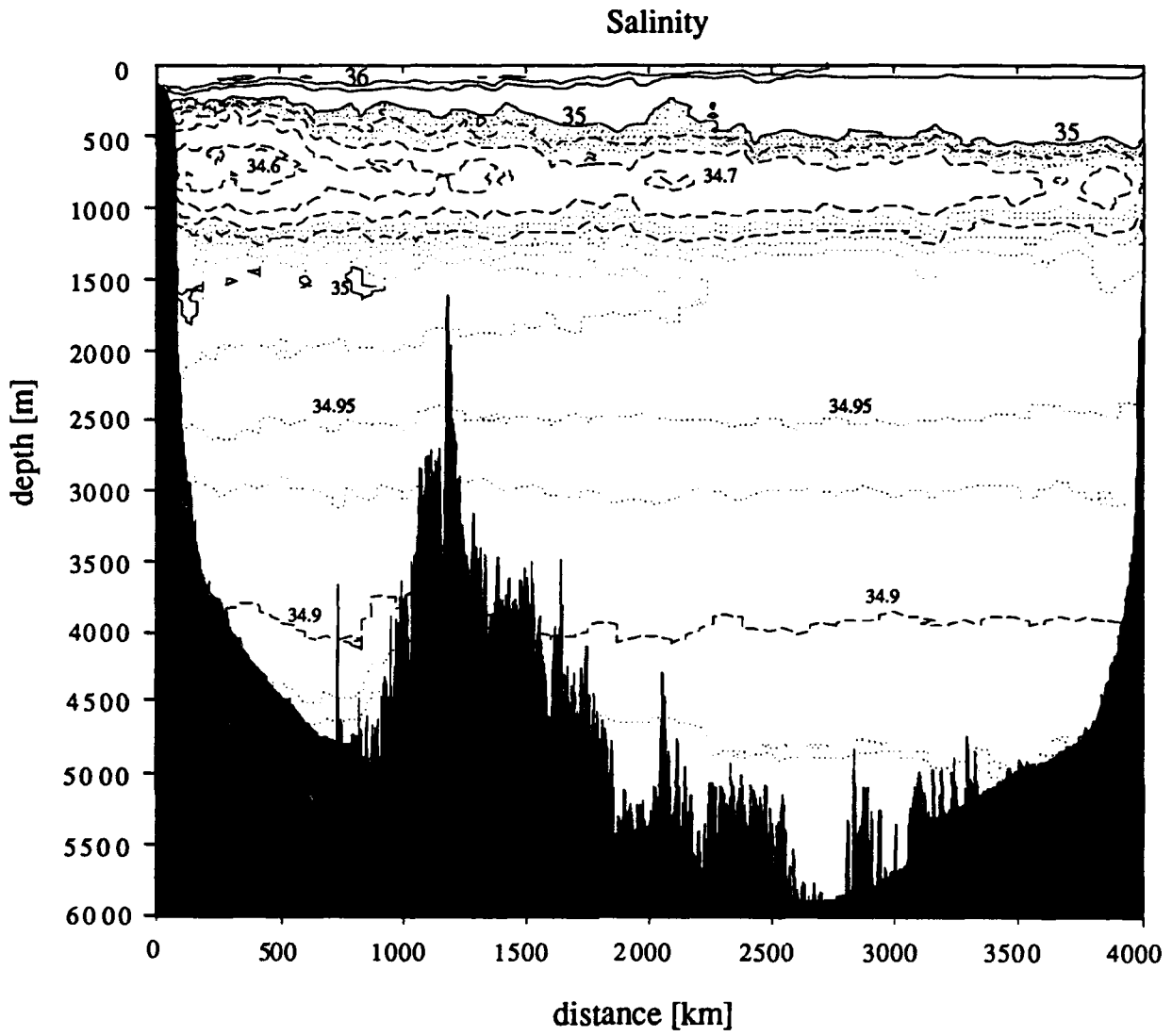


FIG. 7. continued.

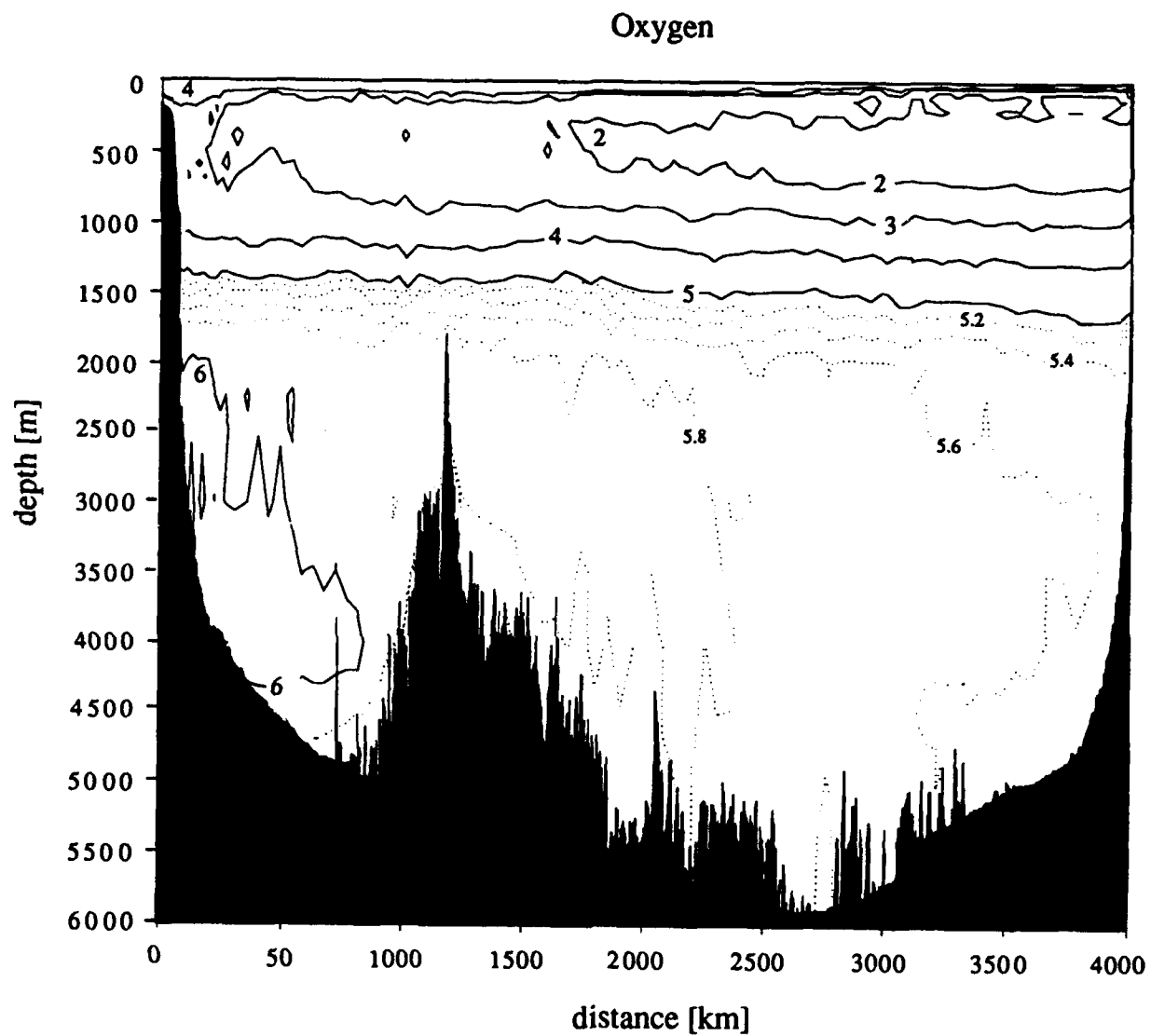


FIG. 7. continued.

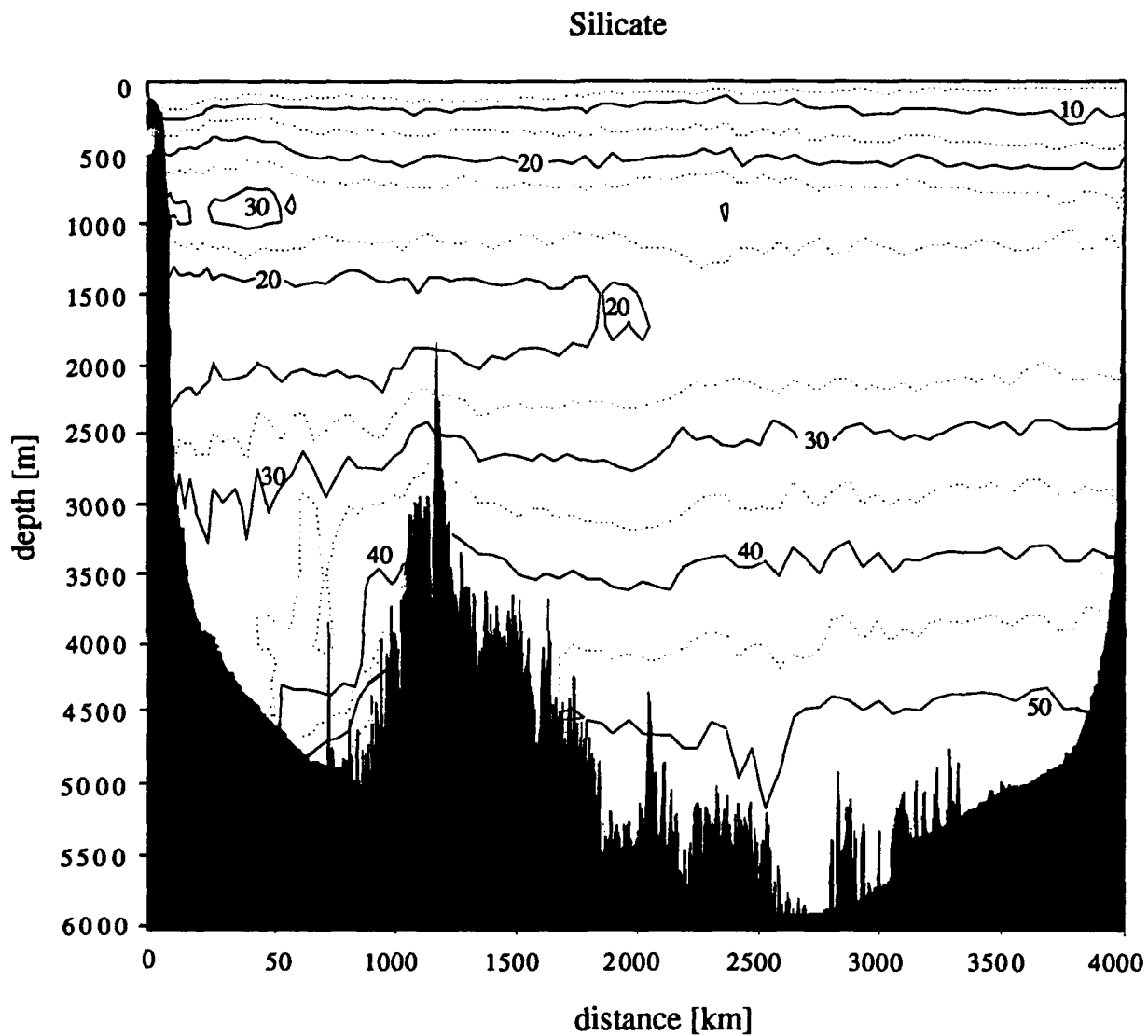


FIG. 7. continued.

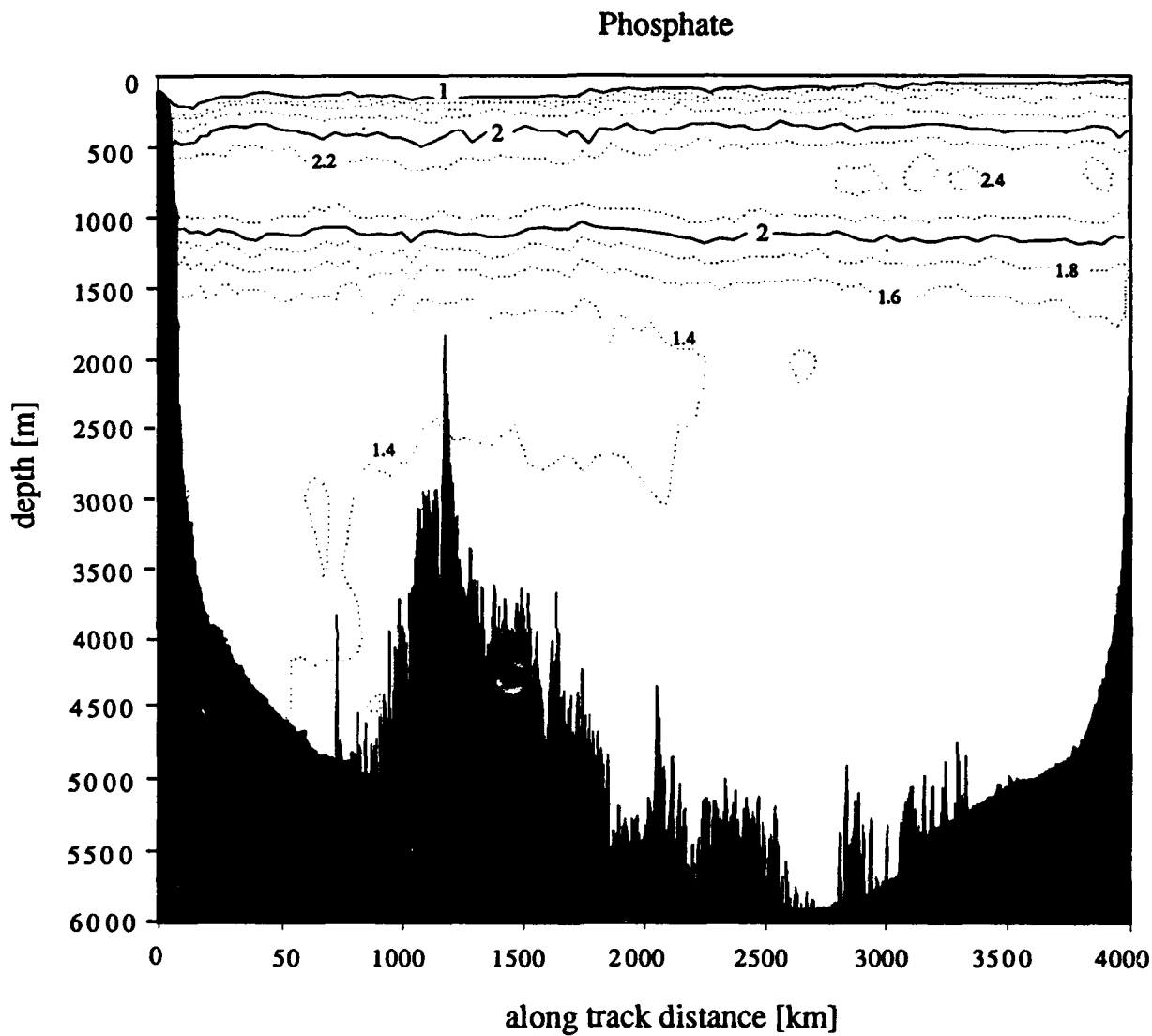


FIG. 7. continued.

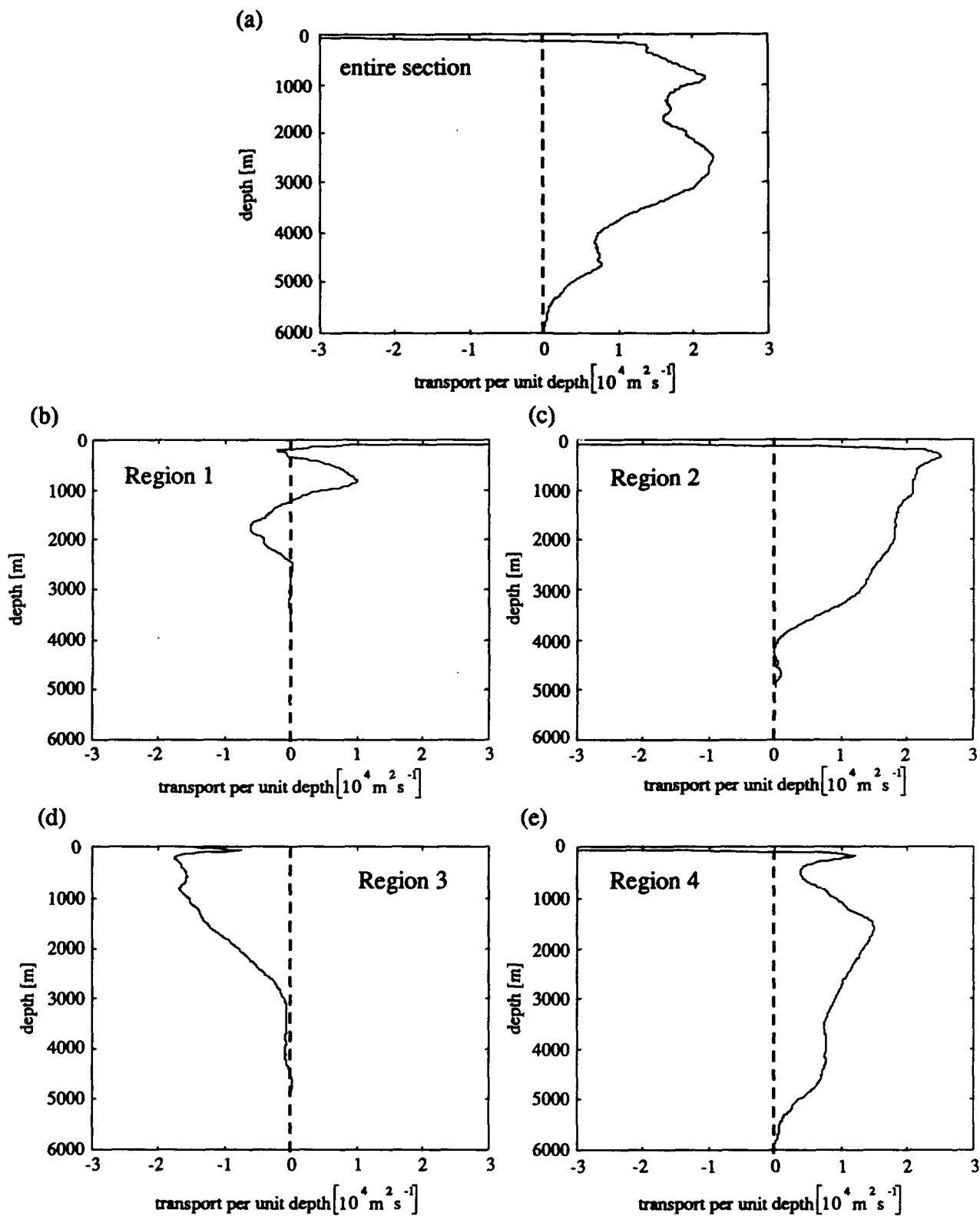


FIG. 8. Transport per unit depth relative to the bottom, for (a) the entire section, (b) Region 1, (c) Region 2, (d) Region 3, and (e) Region 4.

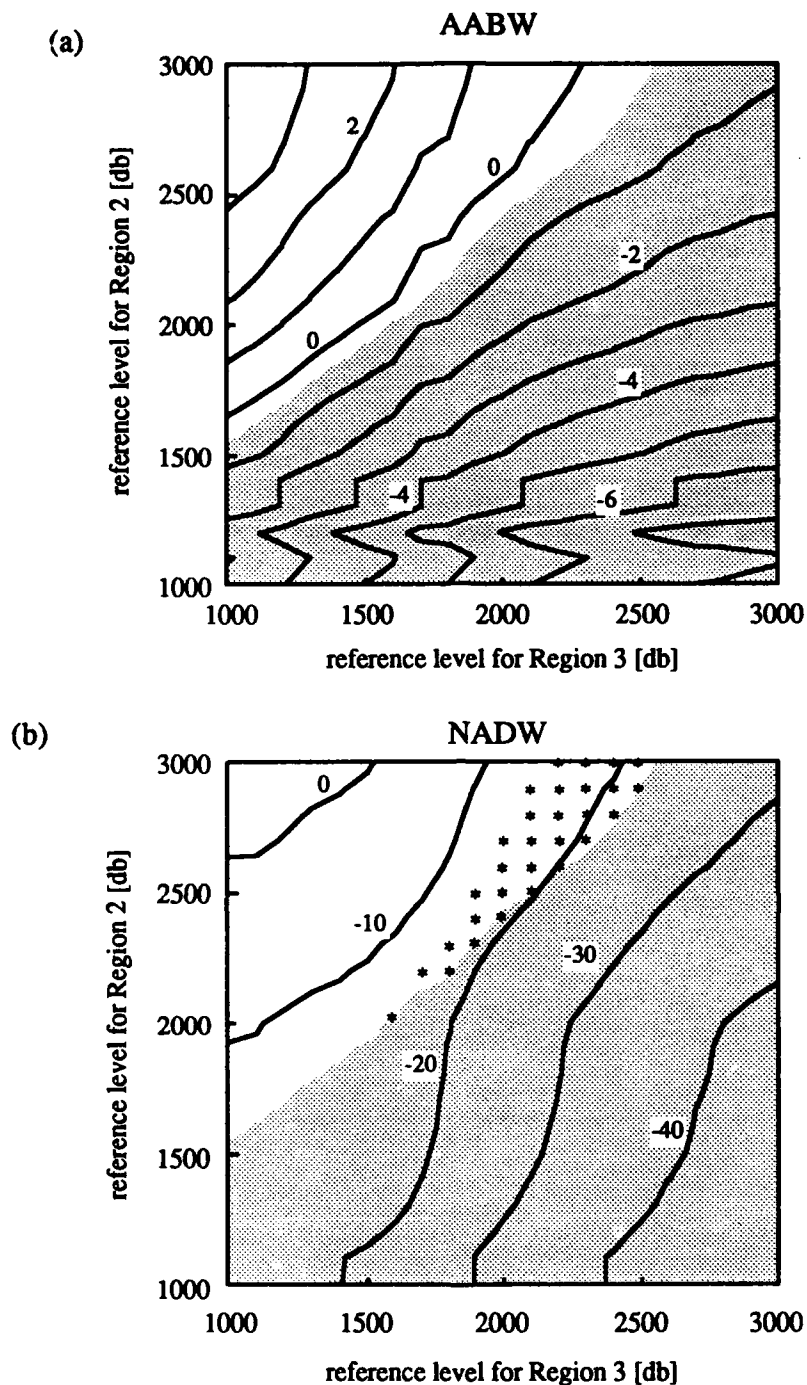


FIG. 9. Contour plots of the western basin transports of (a) AABW and (b) NADW as a function of the reference levels in Regions 2 and 3. The reference level in Region 1 is held constant at 1100 db. Mass is not balanced since we have not yet chosen a reference level for Region 4. The shaded areas in both plots represent the combinations of reference levels which give unrealistically large southward AABW transports within the western basin. Thirty reference level combinations are chosen that give > -0.5 Sv of AABW transport, while maximizing NADW transport. These choices are shown by the asterisks in (b).

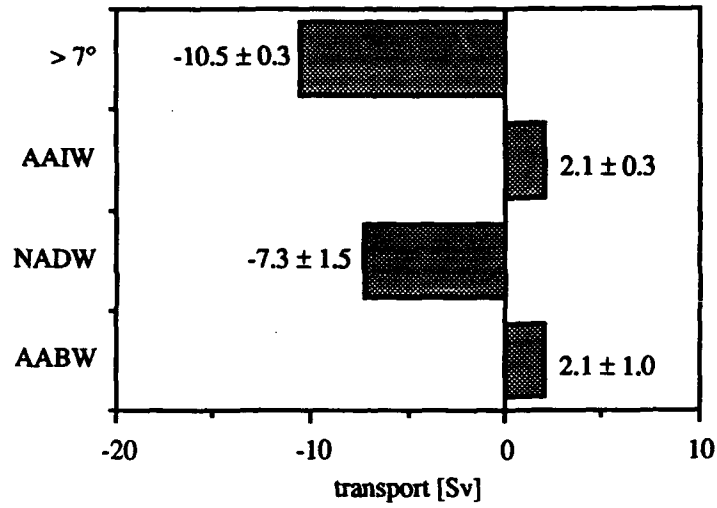


FIG. 10. Mean geostrophic transport in four temperature classes for the 30 reference level combinations described in Table 2 and depicted in Figure 9b. For each combination, mass is balanced by adding a uniform barotropic velocity across the section in order to force the geostrophic transport to balance the sum of the Ekman transport (9.1 ± 1.8 Sv) and the shallow NBC transport ($4.5 \text{ Sv} \pm 1 \text{ Sv}$). Error bars include the uncertainties in the bottom triangle, Ekman, and shallow NBC transports.

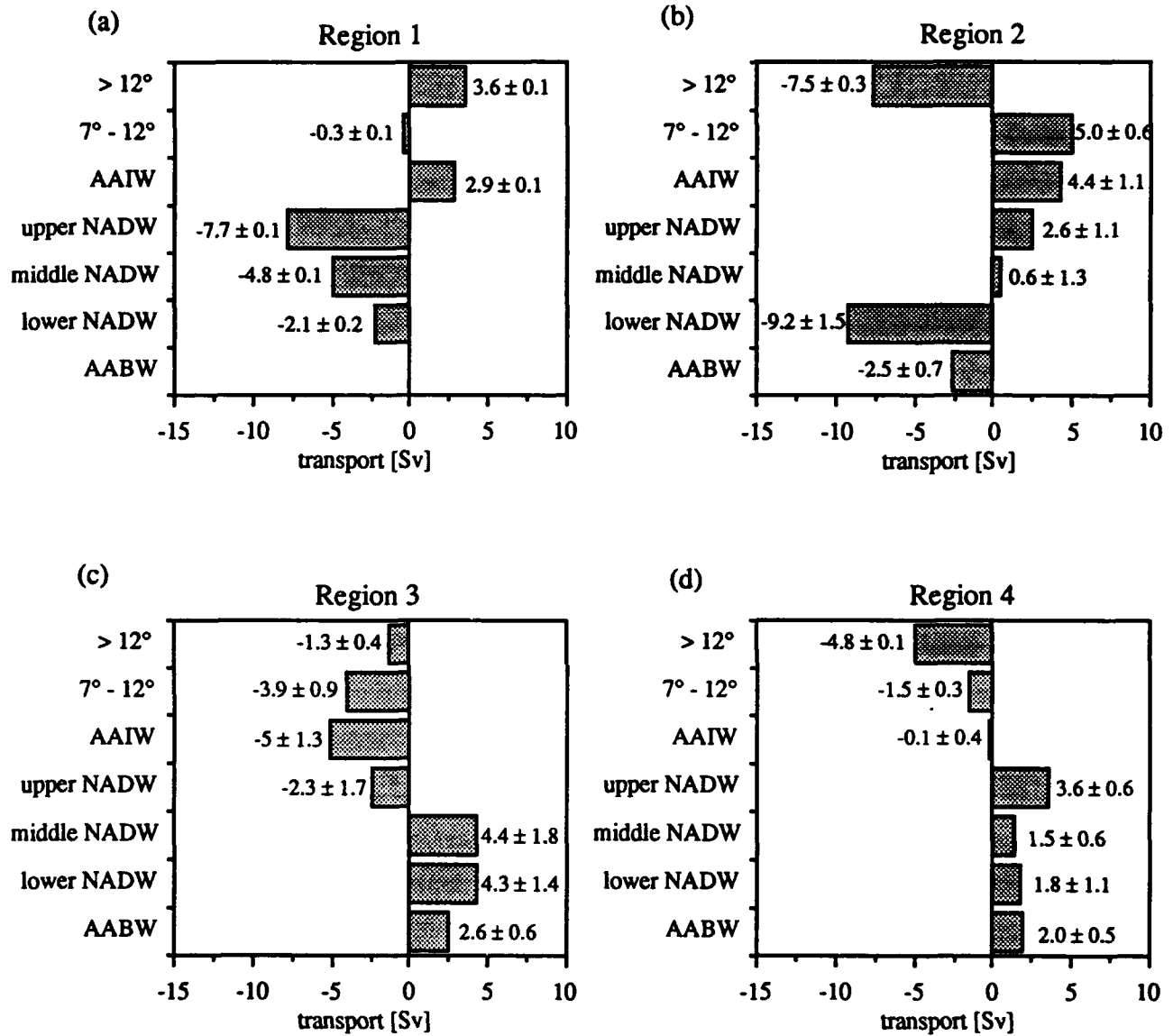


FIG. 11. Geostrophic transport in seven temperature classes for (a) Region 1, (b) Region 2, (c) Region 3, and (d) Region 4.

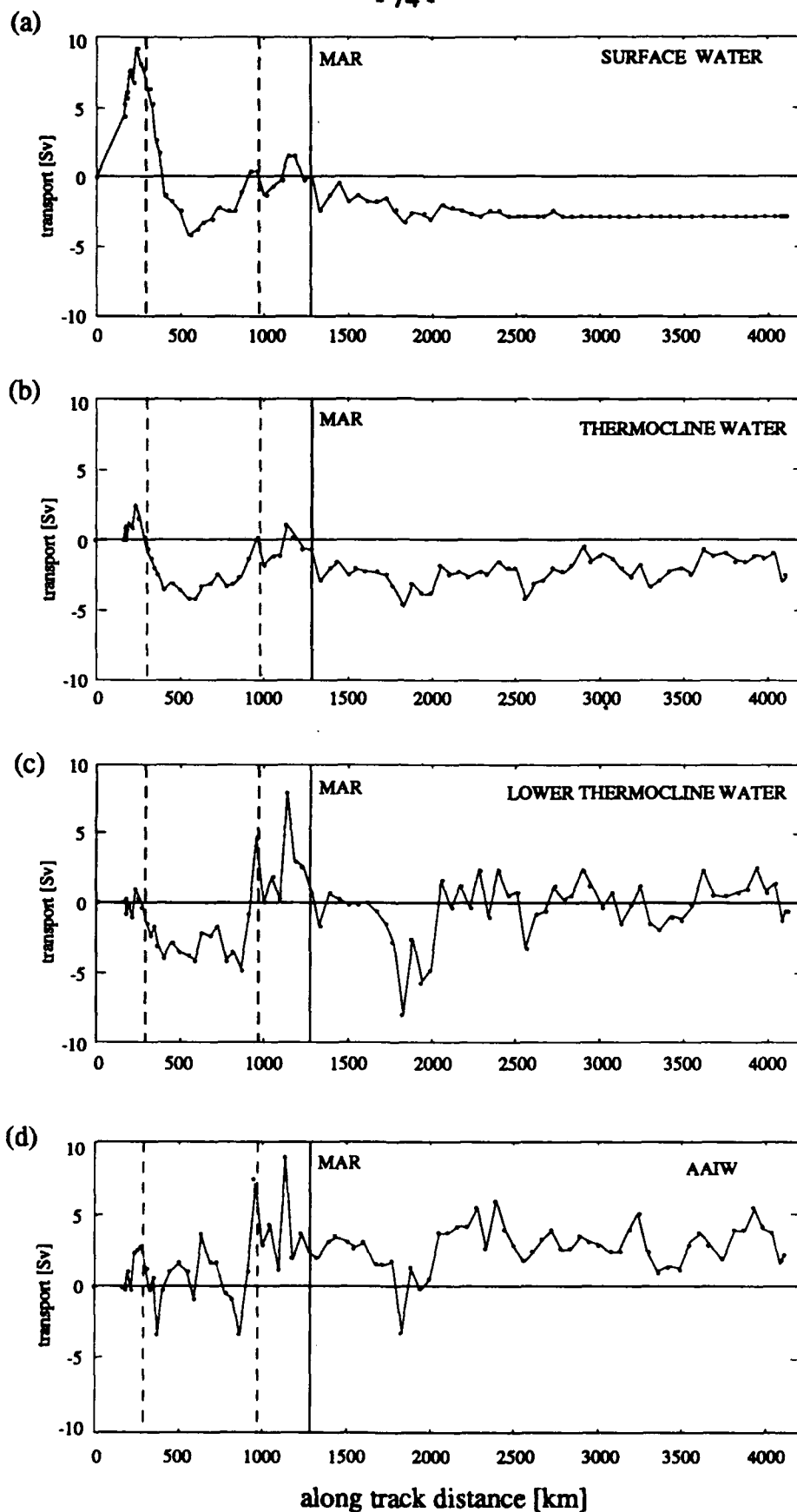


FIG. 12. Transport integrated seaward from the western boundary, as a function of along-track distance for: (a) surface water, including the absolute shallow NBC transport, but *not* the Ekman transport over the remainder of the section, (b) thermocline water, (c) lower thermocline water, (d) AAIW, (e) upper NADW, (f) middle NADW, (g) lower NADW, and (h) AABW. Solid vertical line represents the center of the MAR while the dashed lines indicate the divisions between Regions 1 - 3.

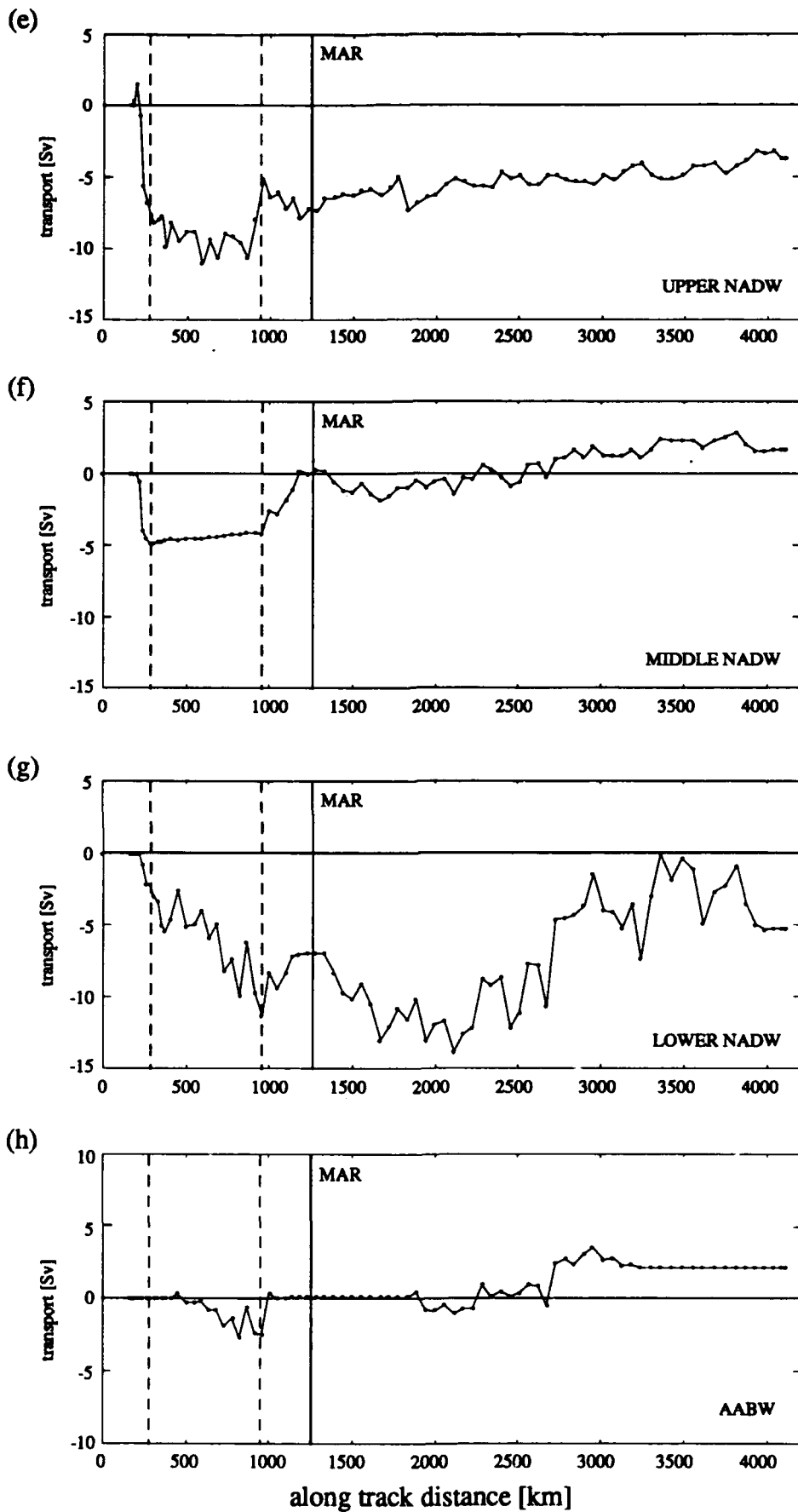


FIG. 12. continued.

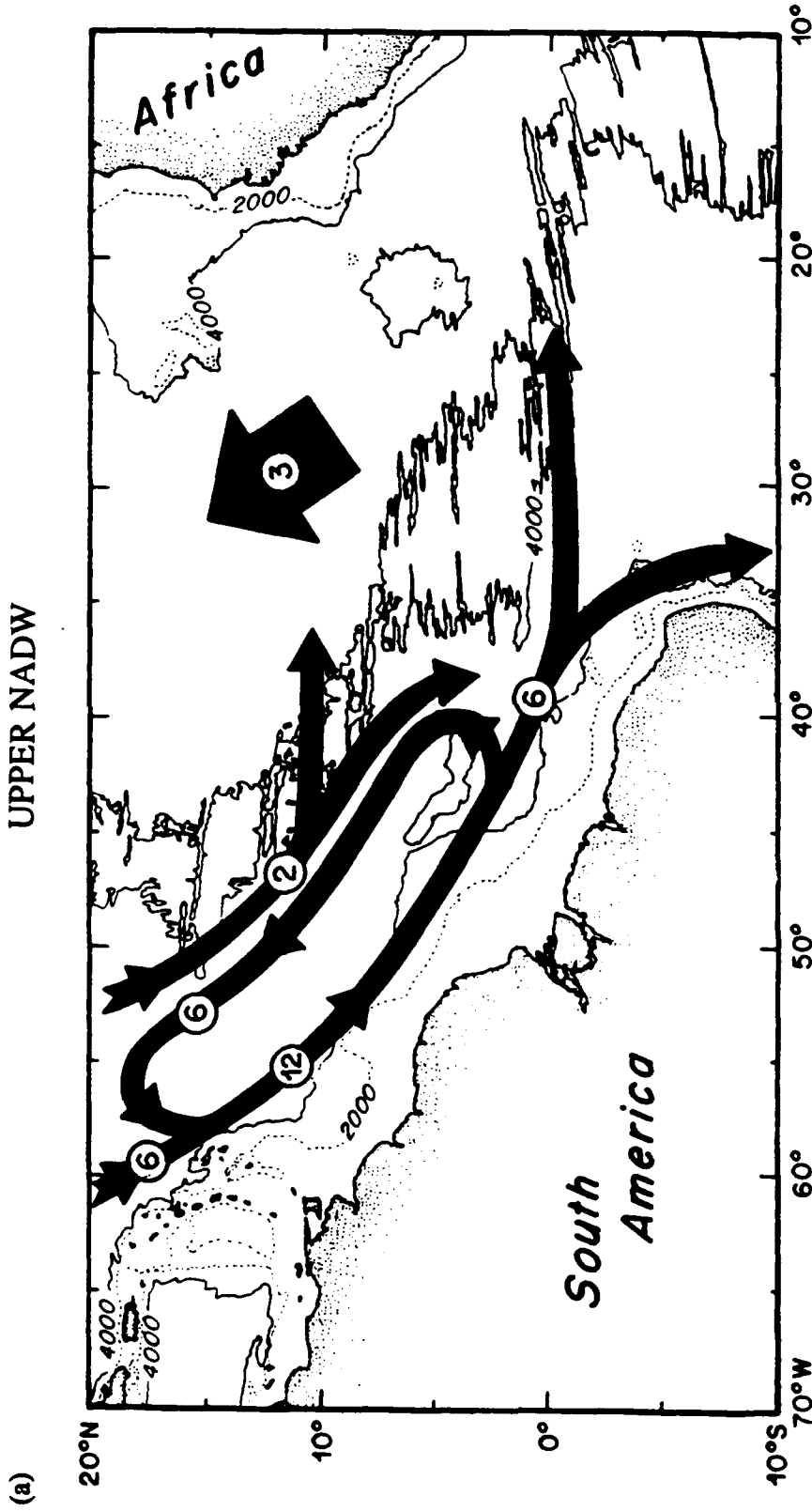


FIG. 13. Schematic circulation patterns in the tropical Atlantic, for: (a) upper NADW, (b) middle NADW, (c) lower NADW, and (d) AABW. The wide arrow in (a) signifies flow evenly distributed throughout the eastern basin.

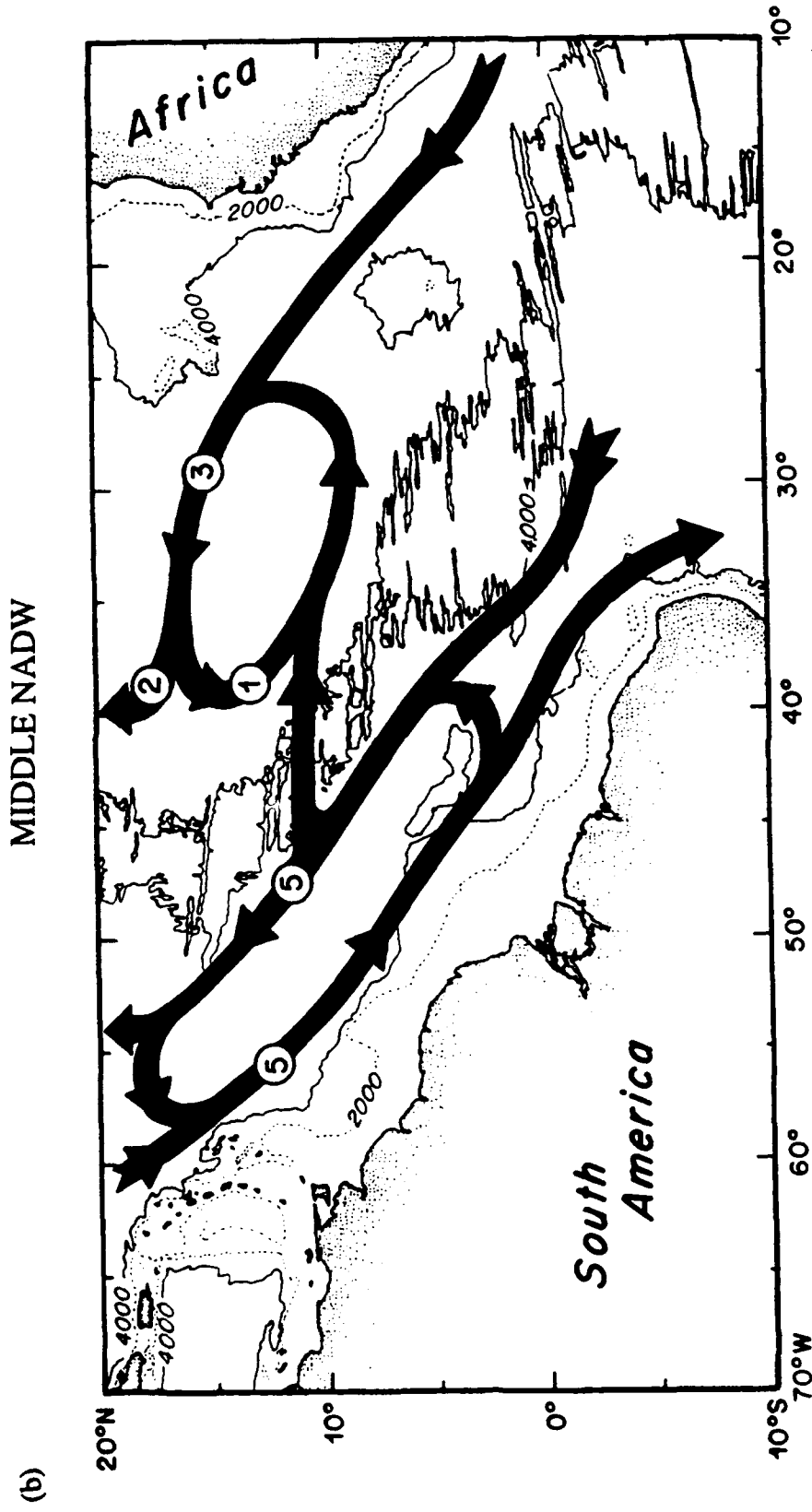


FIG. 13. Continued.

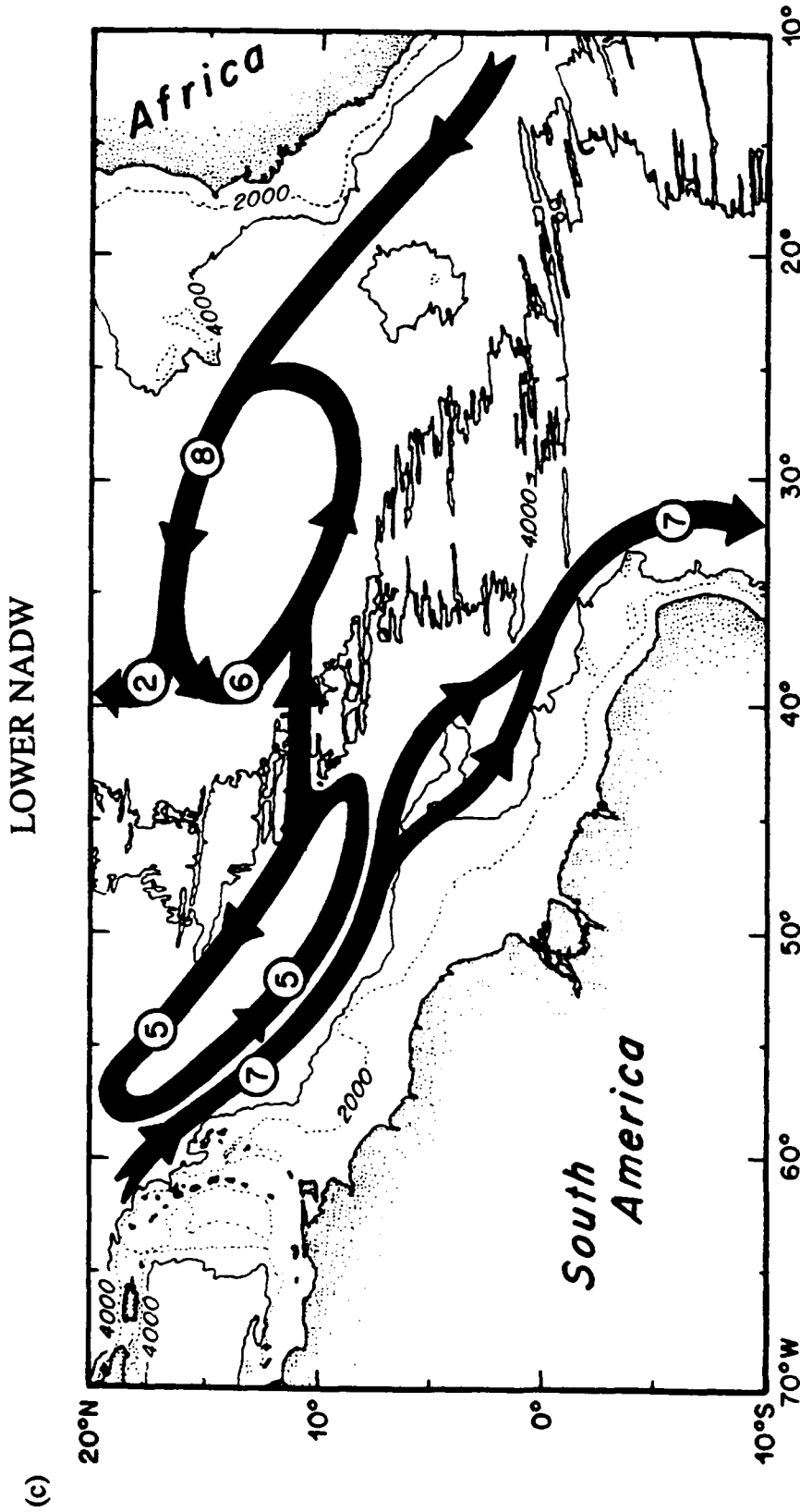


FIG. 13. Continued.

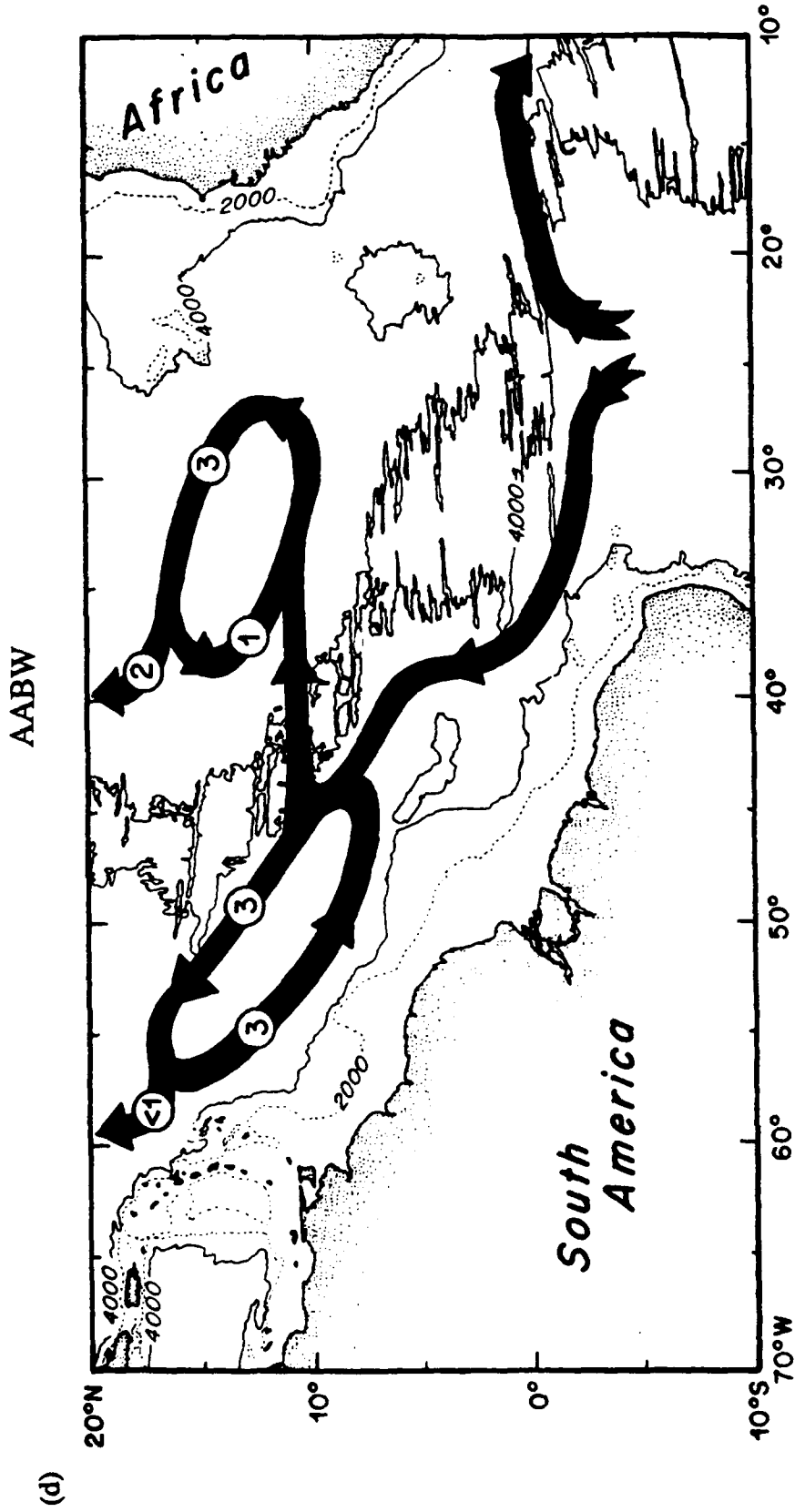


FIG. 13. Continued.

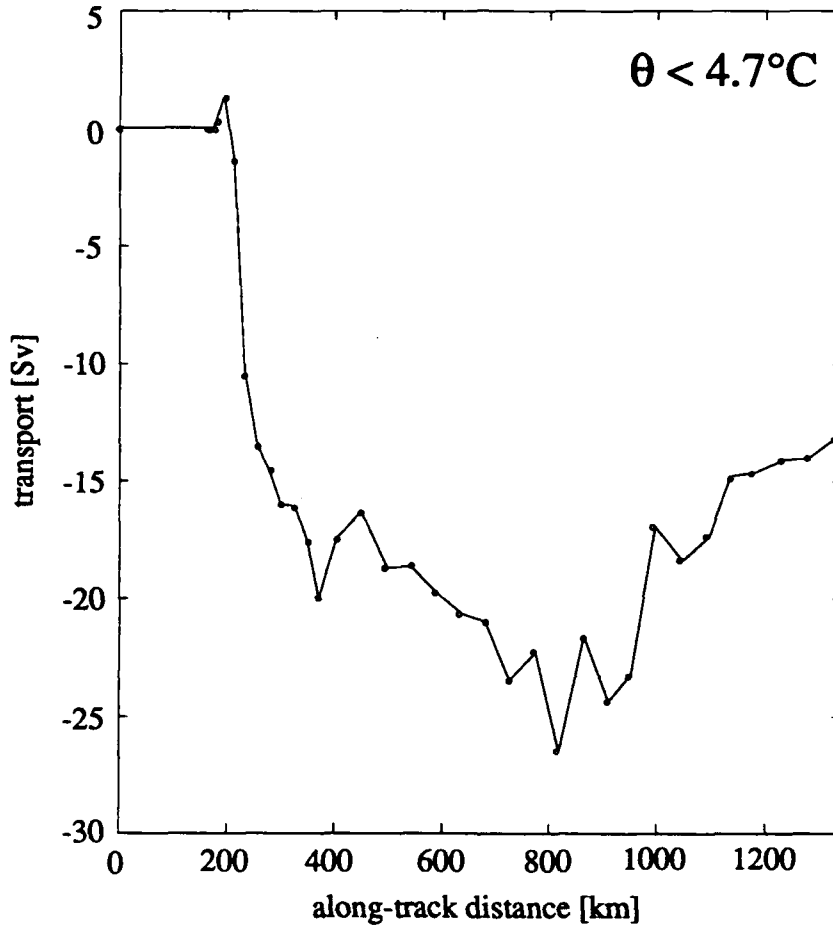


FIG. 14. Transport of $\theta < 4.7^\circ\text{C}$ integrated seaward from the western boundary. The DWBC, defined as flow to the west of the maximum integrated transport of $\theta < 4.7^\circ\text{C}$, transports 26.5 Sv southward. Half of this, 13.2 Sv, recirculates northward along the western flank of the MAR.

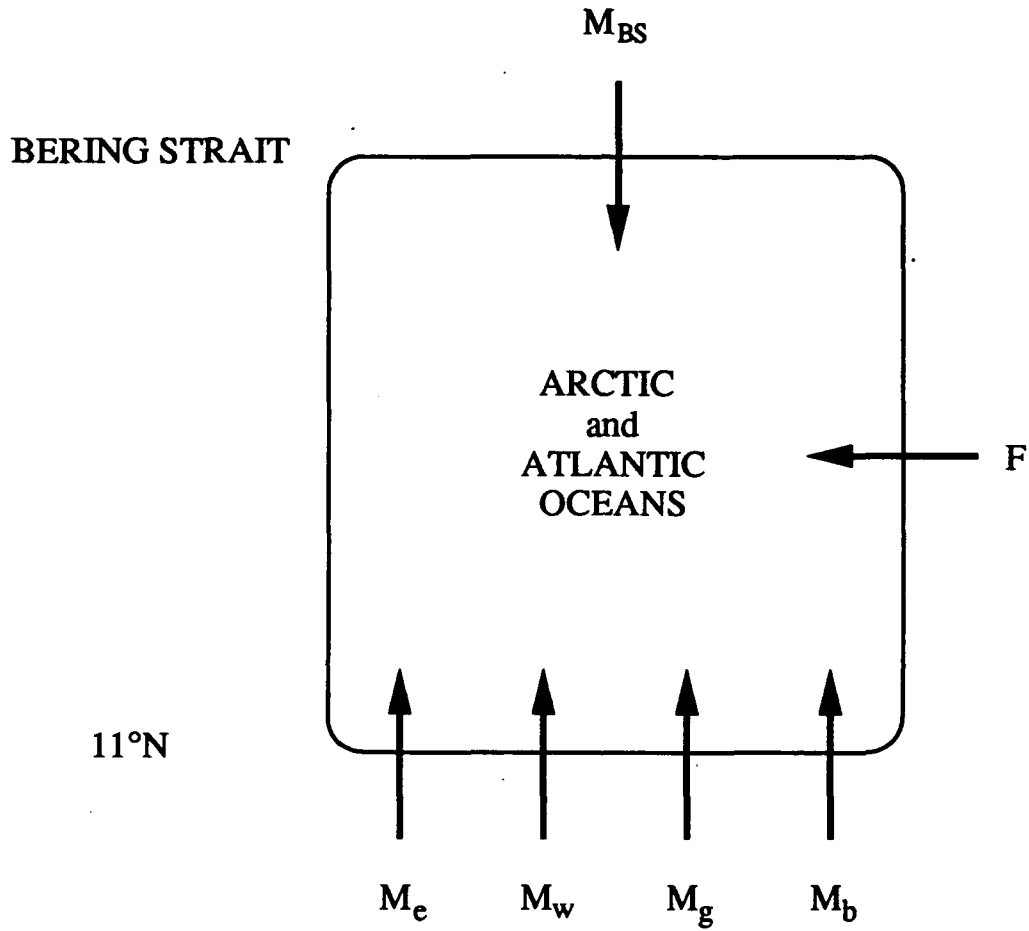


FIG. 15. Mass balance for the region between the Bering Strait and the 11°N section.

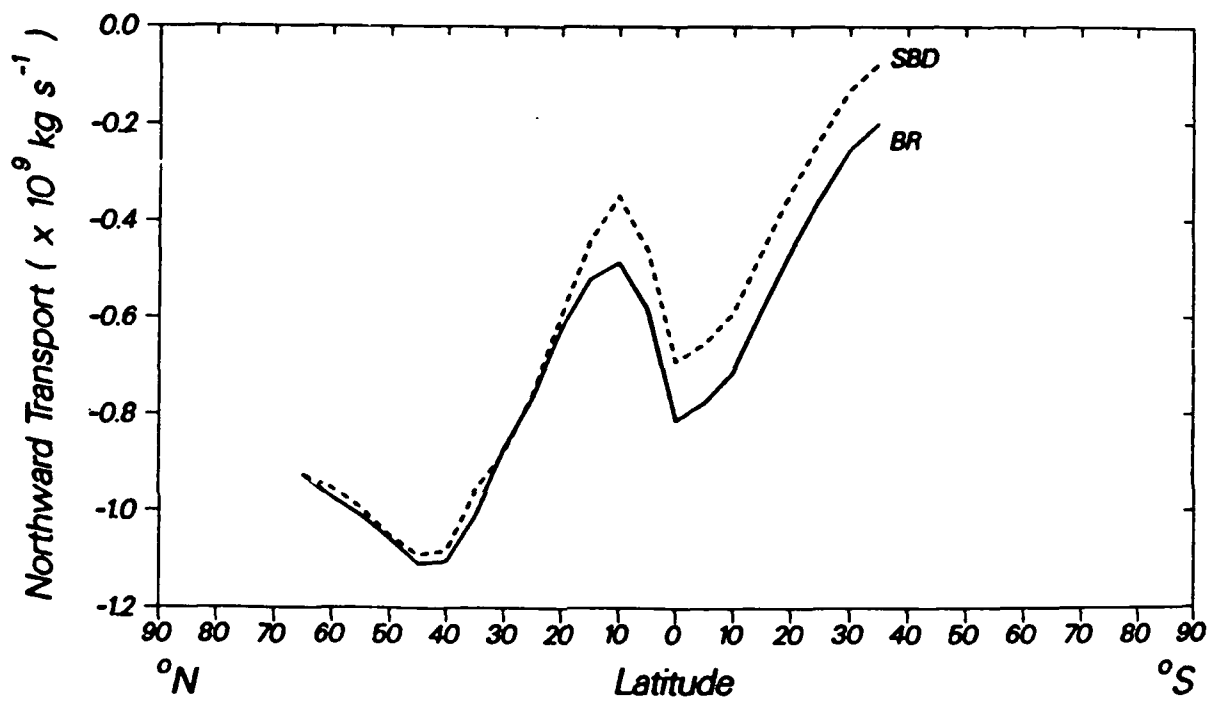


FIG. 16. Indirect estimates of the northward transport of freshwater in the Atlantic Ocean as a function of latitude. Integration using the data of Baumgartner and Reichel (1975) is denoted by BR, while that using the updated data of Schmitt et al. (1989) is denoted by SBD. [Adapted from Wijffels et al. 1992].

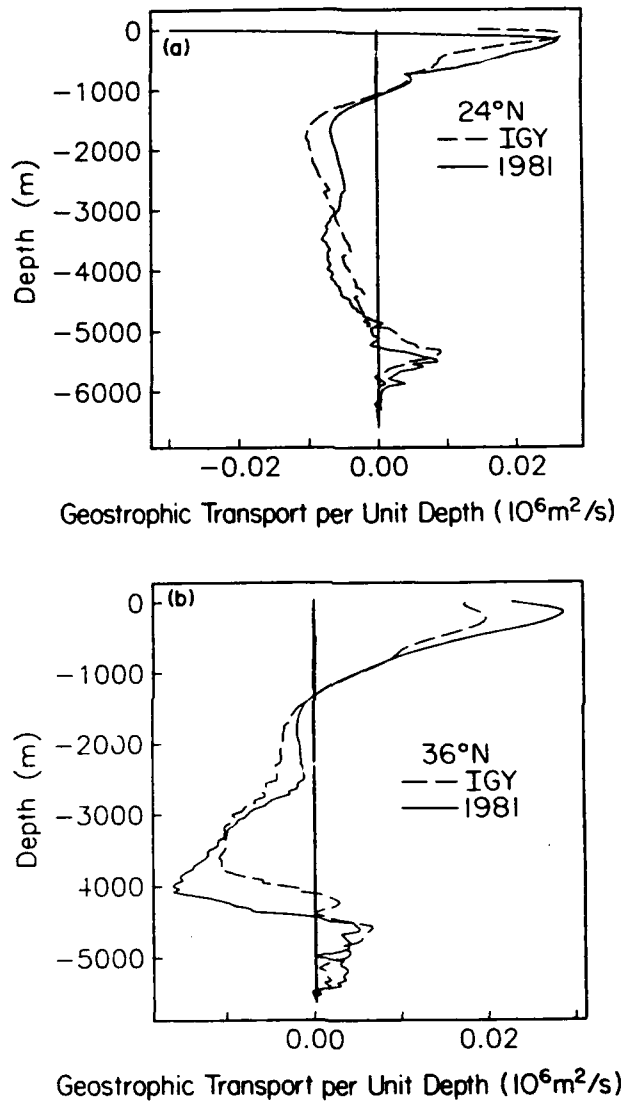
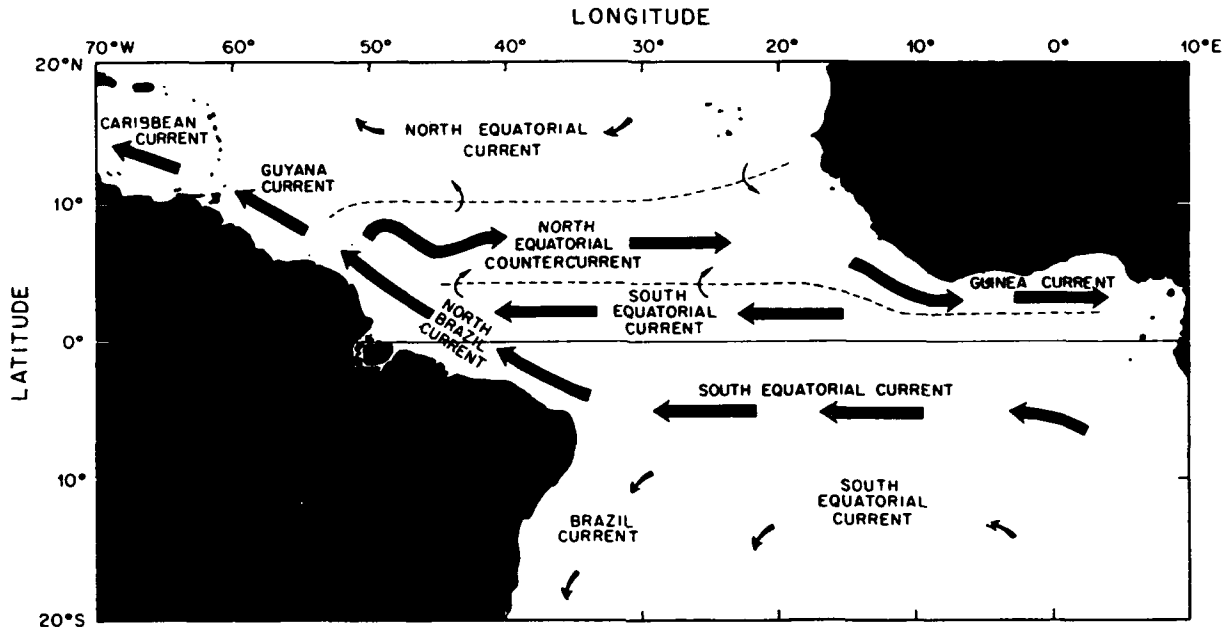


FIG. 17. Geostrophic transport per unit depth based on a traditional reference level calculation across (a) 24°N including the Straits of Florida, and (b) 36°N. [Adapted from Roemmich and Wunsch 1985.]



SCHEMATIC MAP OF CURRENTS IN THE TROPICAL ATLANTIC

FIG. 18. Schematic map showing the major tropical currents between July and September, when the North Equatorial Countercurrent flows swiftly eastward across the Atlantic and into the Guinea Current. From January through June the countercurrent usually disappears, and westward velocities are typically seen in this area. [From Richardson and Walsh 1986.]

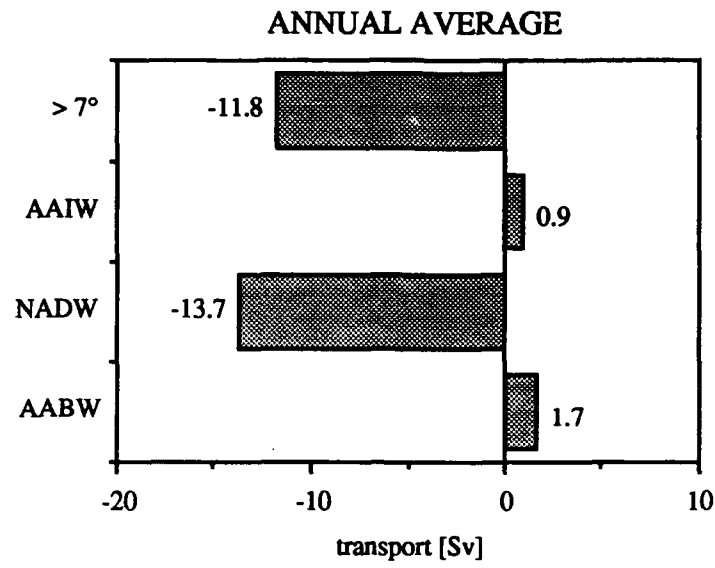


FIG. 19. As in Figure 10, except annual average estimates for the Ekman transport (10 Sv) and the shallow NBC transport (13 Sv) are used.

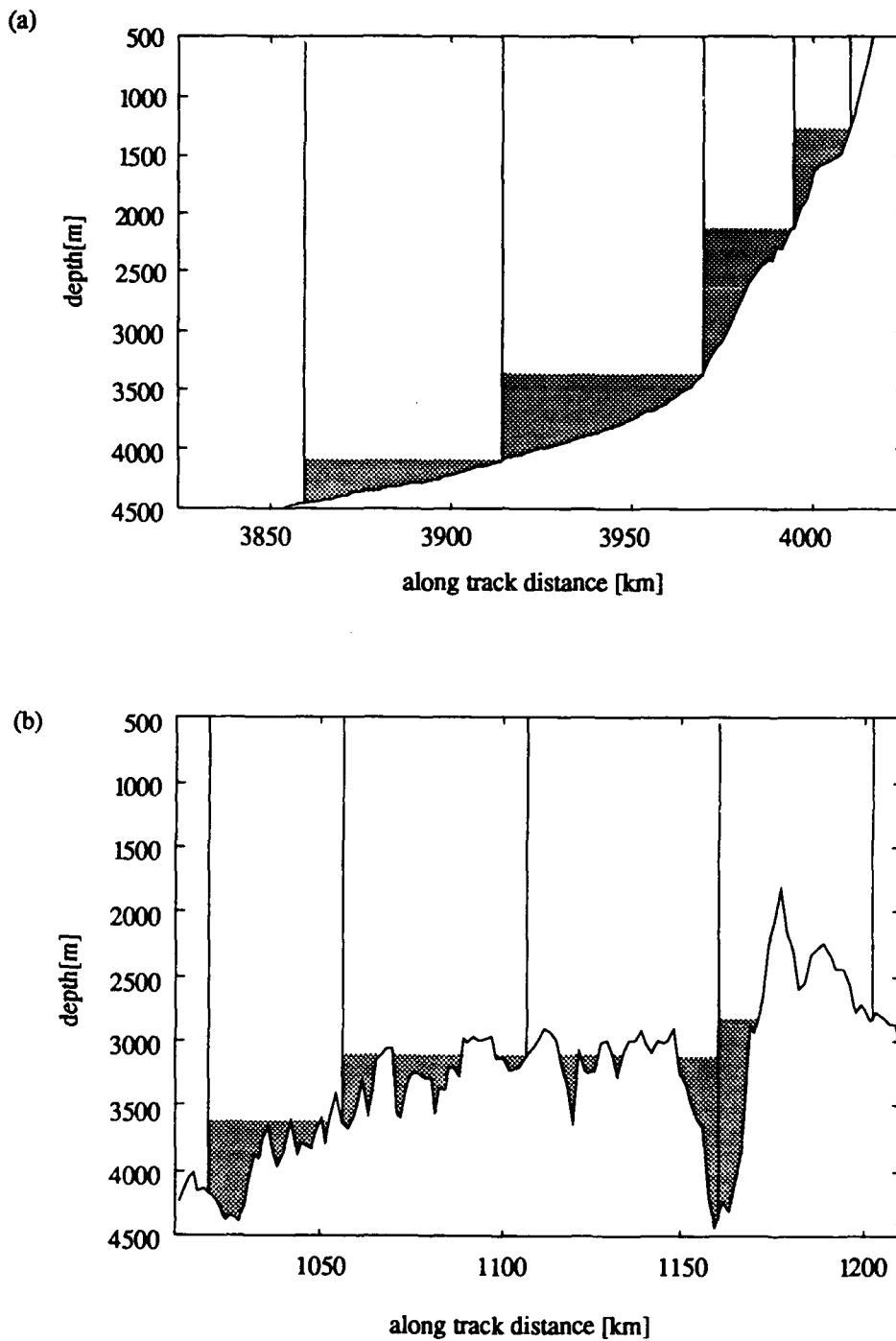


FIG. A1. Five stations overlaid on local topography across two portions of the 11°N section: (a) the eastern continental slope, and (b) the western side of the MAR. Bottom 'triangles' are denoted by shading.

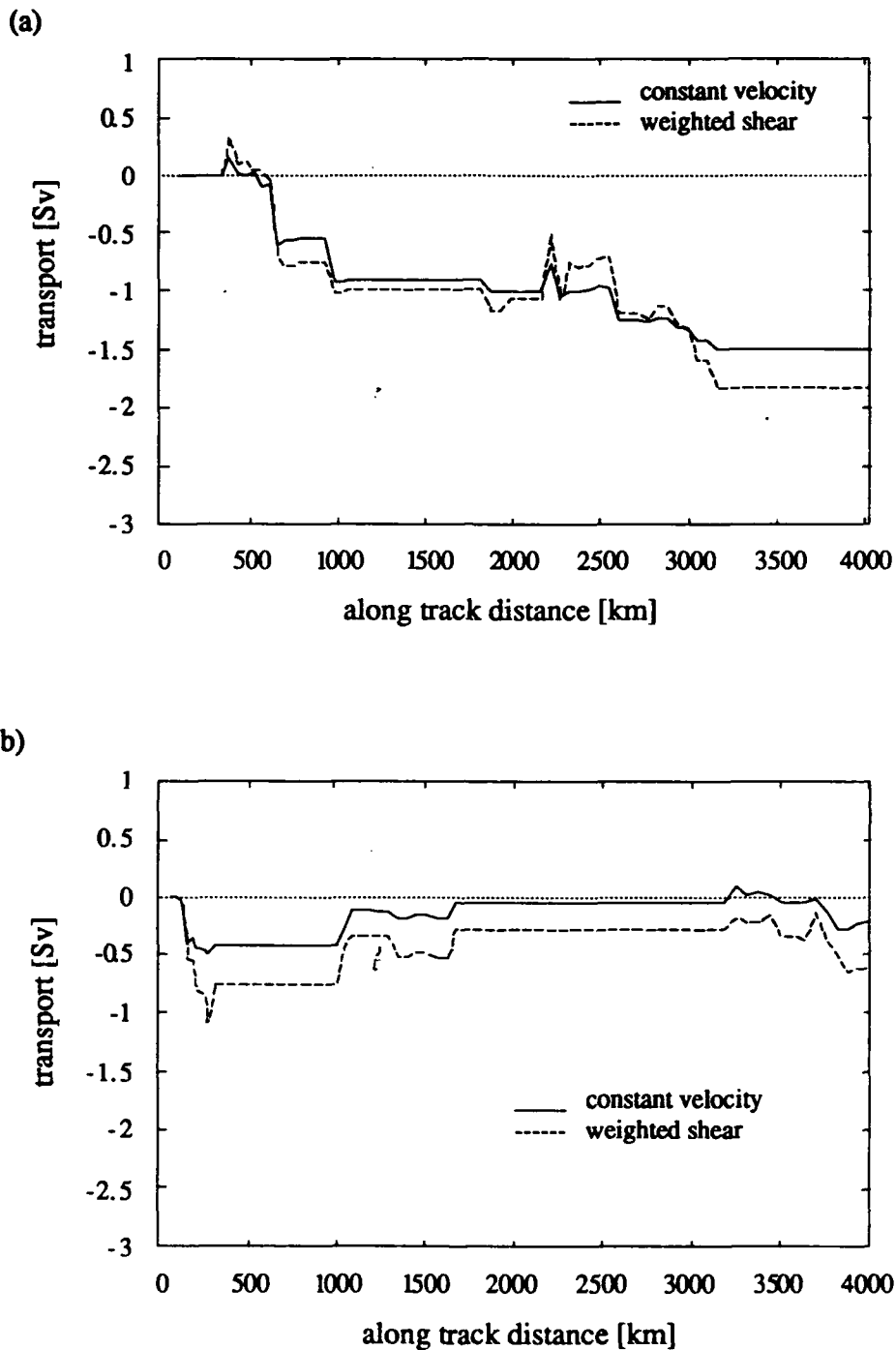


FIG. A2. Bottom triangle transport integrated from west to east computed by means of two different methods, as described in the text. (a) AABW transport ($\theta < 1.8^\circ\text{C}$) (b) lower NADW transport ($1.8^\circ < \theta < 2.4^\circ$). Reference level choices will be described in Section 2c, and shown in Table 2.

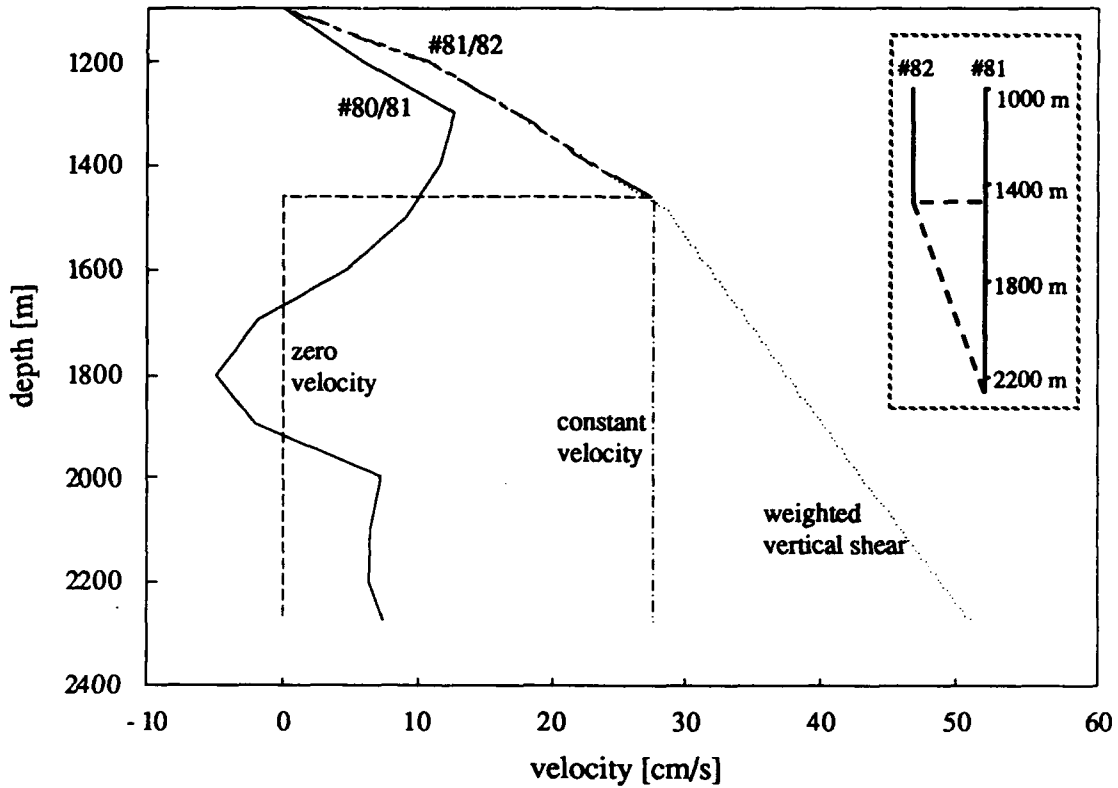


FIG. A3. Velocity profile within the bottom triangle of station pair #81/82 calculated by means of the two extrapolation methods (weighted vertical shear and constant velocity) described in text. Also shown are the velocity profile assuming zero velocity within the bottom triangle, as well as the velocity profile at the same depths for the adjacent station pair #80/81. Since these stations are deeper there is enough information to calculate relative geostrophic velocities and no extrapolation procedure at this depth is necessary. (All velocities are relative to 1100 db; this reference level choice will be defended in Section 2c.)